Title

A nicotinamide phosphoribosyltransferase—GAPDH interaction sustains the stress-induced NMN/NAD+ salvage pathway in the nucleus

Journal

Journal of Biological Chemistry, 295(11)

ISSN

0021-9258

Authors

Grolla, Ambra A
Miggiano, Riccardo
Di Marino, Daniele
et al.

Publication Date

2020-03-01

DOI

10.1074/jbc.ra119.010571

A nicotinamide phosphoribosyltransferase–GAPDH interaction sustains the stress-induced NMN/NAD$^+$ salvage pathway in the nucleus

Received for publication, August 8, 2019, and in revised form, January 16, 2020 Published, Papers in Press, January 27, 2020, DOI 10.1074/jbc.RA119.010571

Ambra A. Grolla[‡1], Riccardo Miggiano[‡1], Daniele Di Marino[§], Michele Bianchi[‡], Alessandro Gori[¶], Giuseppe Orsomando[‖], Federica Gaudino[**], Ubaldina Galli[‡], Erika Del Grosso[‡], Francesca Mazzola[‖], Carlo Angeletti[‖], Martina Guarneri[‡], Simone Torretta[‡], Marta Calabrò[‡], Sara Boumya[‡], Xiaorui Fan[‡‡], Giorgia Colombo[‡], Cristina Travelli[§§], Francesca Rocchio[‡], Eleonora Aronica[¶¶], James A. Wohlschlegel[‡‡], Silvia Deaglio[‖‖], Menico Rizzi[‡], Armando A. Genazzani[‡2], and Silvia Garavaglia[‡3]**

From the [‡]Department of Pharmaceutical Sciences, University of Piemonte Orientale, Largo Donegani 2, 28100 Novara, Italy, the [§]Department of Life and Environmental Sciences, New York-Marche Structural Biology Center (NY-MaSBiC), Polytechnic University of Marche, Via Brecce Bianche, 60131 Ancona, Italy, the [¶]Istituto di Chimica del Riconoscimento Molecolare (ICRM-CNR), via Mario Bianco 9, 20131 Milano, Italy, the [‖]Department of Clinical Sciences (DISCO), Section of Biochemistry, Polytechnic University of Marche, Via Ranieri 67, 60128 Ancona, Italy, the [**]Department of Medical Sciences, University of Turin, Via Nizza 52, 10126 Turin, Italy, the [‡‡]Department of Biological Chemistry, UCLA, Los Angeles, California 90095, [¶¶]Amsterdam UMC, University of Amsterdam, Department of (Neuro)Pathology, Amsterdam Neuroscience, 1001 NK Amsterdam, The Netherlands, the [§§]Department of Pharmaceutical Sciences, University of Pavia, Via Taramelli 12/14, 27100 Pavia, Italy, and the [‖‖]Italian Institute for Genomic Medicine, Via Nizza 52, 10126 Turin, Italy

Edited by John M. Denu

All cells require sustained intracellular energy flux, which is driven by redox chemistry at the subcellular level. NAD$^+$, its phosphorylated variant NAD(P)$^+$, and its reduced forms NAD(P)/NAD(P)H are all redox cofactors with key roles in energy metabolism and are substrates for several NAD-consuming enzymes (*e.g.* poly(ADP-ribose) polymerases, sirtuins, and others). The nicotinamide salvage pathway, constituted by nicotinamide mononucleotide adenylyltransferase (NMNAT) and nicotinamide phosphoribosyltransferase (NAMPT), mainly replenishes NAD$^+$ in eukaryotes. However, unlike NMNAT1, NAMPT is not known to be a nuclear protein, prompting the question of how the nuclear NAD$^+$ pool is maintained and how it is replenished upon NAD$^+$ consumption. In the present work, using human and murine cells; immunoprecipitation, pulldown, and surface plasmon resonance assays; and immunofluorescence, small-angle X-ray scattering, and MS-based analyses, we report that GAPDH and NAMPT form a stable complex that is essential for nuclear translocation of NAMPT. This translocation furnishes NMN to replenish NAD$^+$ to compensate for the activation of NAD-consuming enzymes by stressful stimuli induced by exposure to H_2O_2 or *S*-nitrosoglutathione and DNA damage inducers. These results indicate that by forming a complex with GAPDH, NAMPT can translocate to the nucleus and thereby sustain the stress-induced NMN/NAD$^+$ salvage pathway.

All cells require sustained and incessant fluxes of energy, which are accomplished through complex redox chemistry performed at the subcellular level. In this, pyridine dinucleotides (NAD$^+$/NADH and NADP$^+$/NADPH) are key players, employed in at least 488 human metabolic reactions (1). The diverse metabolic functions of pyridine nucleotides are possible due to the specificity and compartmentalization of cellular enzymes that utilize them (2). Pyridine nucleotides regulate basal metabolism through their co-enzymatic function in redox reactions underlying essential bioenergetic pathways (3). However, they are also intimately involved in signaling pathways (2–5). NAD$^+$ is a rate-limiting substrate for mono- and poly-ADP-ribose transferases (including poly(ADP-ribose) polymerases; PARPs)[4] (6), cyclic ADP-ribose synthases (CD38 and CD157) (7), SARM1 (8), and sirtuins (9). The above sustain the need of a continuous regeneration of NAD$^+$ cofactor to rapidly restore the functionality of NAD-consuming enzymes (10). In this context, the nicotinamide-salvaging biosynthetic route appears to be the main contributor to maintaining NAD home-

This work was supported in part by Associazione Italiana per la Ricerca sul Cancro (AIRC) Grant IG2018 21842 (to A. A. Genazzani), by PRIN 2017 CBNCYT from the Italian Ministry of Health (to A. A. Genazzani), by Fondazione Umberto Veronesi Grant 2018 (to A. A. Genazzani), and by a SIF-Merck scholarship (to A. A. Genazzani), and Università del Piemonte Orientale Grant FAR 2015 (to S. G.). The authors declare that they have no conflicts of interest with the contents of this article.

This article contains Tables S1 and S2 and Figs. S1–S9.

The proteomics data of the MS experiments are available from the MassIVE data repository with the data set identifier MSV000084426.

[1] Both authors equally contributed to this work.

[2] To whom correspondence may be addressed. E-mail: armando.genazzani@uniupo.it.

[3] To whom correspondence may be addressed. E-mail: silvia.garavaglia@uniupo.it.

[4] The abbreviations used are: PARP, poly(ADP-ribose) polymerase; NAMPT, nicotinamide phosphoribosyltransferase; NMNAT, nicotinamide mononucleotide adenylyltransferase; GAPDH, glyceraldehyde-3-phosphate dehydrogenase; IP, immunoprecipitation(s); SPR, surface plasmon resonance; SEC, size-exclusion chromatography; SAXS, small-angle X-ray scattering; PDB, Protein Data Bank; XL, cross-linked; GSNO, *S*-nitrosoglutathione; NLS, nuclear localization sequence; cpVenus, circularly permutated Venus; MTT, 3-(4,5-dimethylthiazol-2-yl)-2,5-diphenyltetrazolium bromide; G3P, glyceraldehyde 3-phosphate; Mo, mouse; Rb, rabbit.

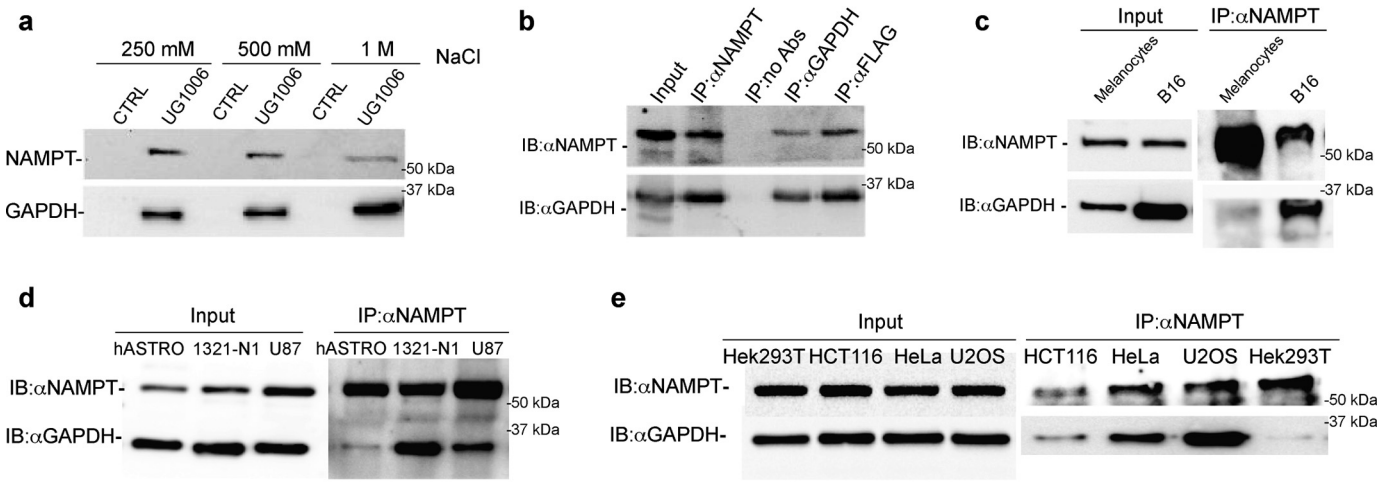

Figure 1. NAMPT interacts with GAPDH in cells. *a*, affinity chromatography with UG1006-conjugated beads pulled down NAMPT and GAPDH in B16 melanoma cells in stringent salt concentrations. *b*, IP with mouse αNAMPT or αGAPDH immunoprecipitated GAPDH or NAMPT, respectively, revealed with αRabbit, in B16 cells. The *last lane* represents an IP with αFLAG-conjugated beads in B16 overexpressing FLAG-NAMPT. *c*, IP with αNAMPT in human adult melanocytes *versus* B16 melanoma cells. *d*, IP with αNAMPT in human fetal astrocytes (*hASTRO*) *versus* human astrocytoma cells (*1321-N1*) and human glioblastoma cells (*U87*). *e*, IP with αNAMPT in the indicated cell lines. *IB*, immunoblotting.

ostasis (11, 12). Nicotinamide phosphoribosyltransferase (NAMPT, PBEF, visfatin, EC 2.7.7.1) is the rate-limiting enzyme of this pathway and catalyzes the production of NMN from nicotinamide and phosphoribosyl pyrophosphate in the cytosol (13, 14). Then NMN is converted into NAD$^+$ by nicotinamide mononucleotide adenylyltransferase (NMNAT), which exists in three different isoforms: nuclear (NMNAT1), cytosolic (NMNAT2), and mitochondrial (NMNAT3) (15). Given its rate-limiting role, both cellular NAD$^+$ levels and the activity of NAD-consuming enzymes are indirectly controlled by NAMPT that exists as an intracellular and extracellular form (16, 17). The intracellular localization of NAMPT is cytosolic, although there are reports that it may also be localized in the nucleus (18, 19) and in the mitochondria (20). Interestingly, Svoboda *et al.* (19) have recently demonstrated that the presence of NAMPT in the nucleus is strictly dependent on the cell cycle, suggesting that there is a need for nuclear NAD$^+$ surges for cell proliferation. Moreover, the presence of PARPs and sirtuins implies that nuclear NAD$^+$ replenishment is required, bypassing the topological paradox by which NMNAT1 and NAMPT are segregated by the nuclear envelope. Whereas it is likely that NMN may diffuse to the nucleus, it would appear counterintuitive that the enzymes of the salvage pathway are separated by the nuclear envelope.

In the present work, we show that glyceraldehyde-3-phosphate dehydrogenase (GAPDH; EC 1.2.1.12) shuttles NAMPT to the nucleus in stress conditions, providing the mechanism by which cells are able to produce NMN in different compartments to maintain NAD homeostasis but also contributing further evidence that GAPDH is significantly more than just a housekeeping glycolytic enzyme (21).

Results

NAMPT and GAPDH interact in cells, forming a stable complex

To selectively capture NAMPT tight interactors from cells, we generated a microbead system built up on a potent NAMPT inhibitor, UG1006, with an IC_{50} of ~200 nM on the recombinant protein, conjugated to Sepharose beads (supporting information). We observed that, in B16 murine melanoma cell lysate, the eluate of UG1006-coupled beads contained both NAMPT and GAPDH. This occurred in stringent salt conditions (250 mM to 1 M NaCl) and did not occur when uncoupled control beads were used (Fig. 1*a*). To investigate this, we performed immunoprecipitations (IP) with αNAMPT, αGAPDH, or αFLAG in B16 cell lysates overexpressing FLAG-NAMPT. As shown in Fig. 1*b*, αGAPDH pulled down NAMPT and αNAMPT, and αFLAG pulled down GAPDH. Superimposable results were obtained using three different commercial αNAMPT and two different αGAPDH (data not shown). Moreover, shotgun proteomics LC-MS/MS analysis of the proteins immunoprecipitated by an αGFP in lysates from B16 cells overexpressing GFP-NAMPT confirmed the presence of GAPDH with 25 MS/MS spectral counts. Control antibodies, such as Bcl10 and HSP90, did not pull down either GAPDH or NAMPT in B16 lysates. Given that B16 cells are melanoma cells, we also analyzed whether the interaction occurred in primary cells of the same origin. In melanocytes, we did not appreciate the same intensity of complex formation (Fig. 1*c*). We also tested whether the complex occurred in other tumoral cells. The complex is evident in astroglioma (1321-N1) and glioblastoma (U87) cell lines (Fig. 1*d*), and again it is significantly less evident in primary human astrocytes (hASTRO). Last, we tested three epithelial cancer cell lines (HCT116, HeLa, and U2OS cells), and the complex was again significantly more intense compared with epithelial HEK293T cells (Fig. 1*e*). The complex formation is therefore generalizable in eukaryotic cells. Whereas our data might also suggest that NAMPT/GAPDH overexpression and/or some specific tumoral conditions might influence the complex formation, this cannot be ascertained at present.

To determine whether there was a direct interaction between GAPDH and NAMPT, we produced a recombinant NAMPT bearing a His_6 tag and a GAPDH protein bearing an easily removable GST tag. Pulldown experiments using these recom-

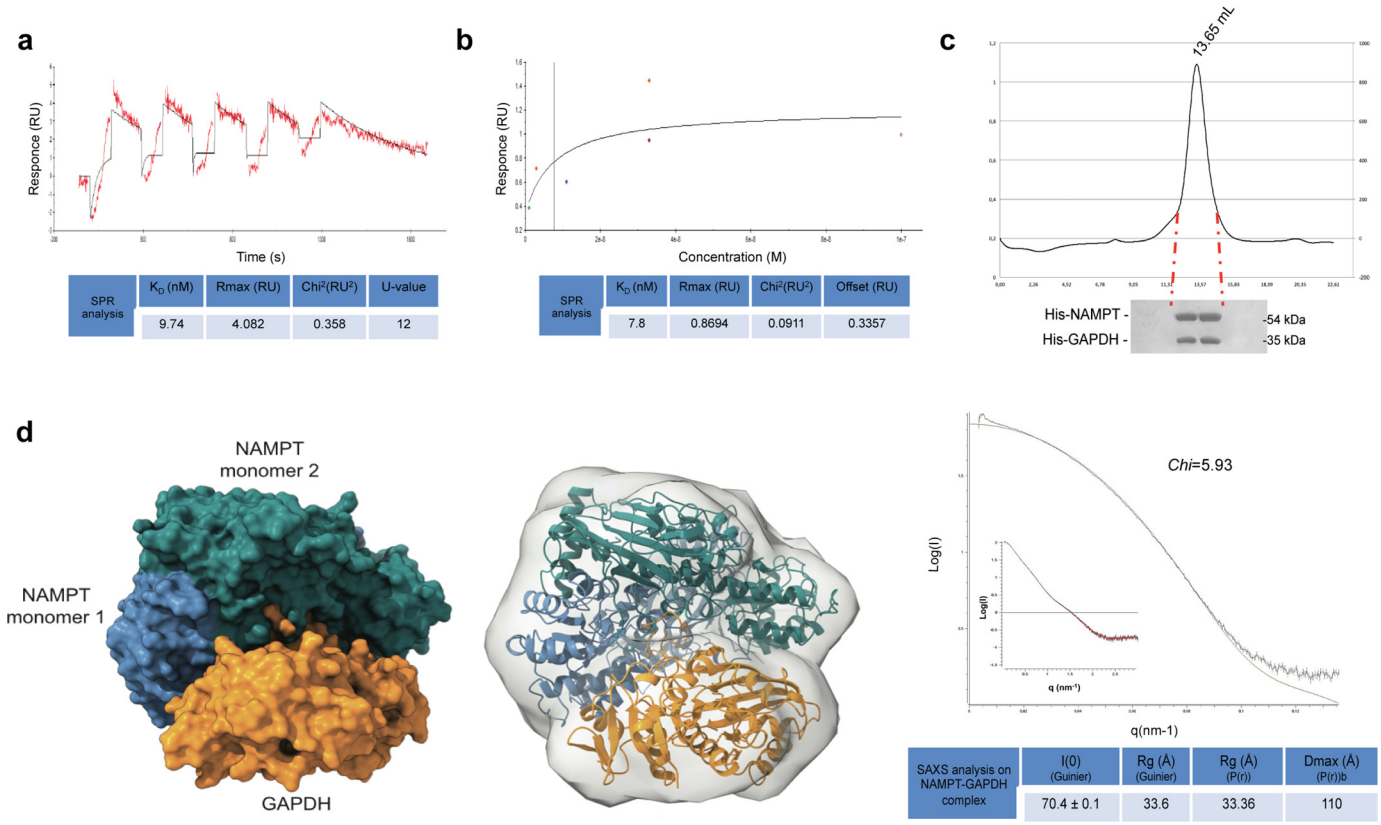

Figure 2. Biochemical and structural analysis of the NAMPT-GAPDH complex. *a*, SPR-based single-cycle kinetics analysis of NAMPT-GAPDH interaction. 0.12, 0.37, 1.11, 3.33, and 10 μM GAPDH solutions were injected onto a CM5 chip coated with NAMPT protein immobilized through an anti-His antibody. *b*, steady-state affinity analysis of SPR-based multiple-cycle kinetics of GAPDH-NAMPT interaction. 1.2, 3.7, 11, 33, and 100 nM NAMPT solutions were injected onto a CM5 chip coated with GAPDH protein immobilized through amine coupling. *c*, SEC chromatogram and relative SDS-PAGE analysis of the eluted fractions corresponding to the peak of the absorbance at 280 nm. *d*, *left*, *surface representation* of the model of NAMPT$_2$-GAPDH complex. *Center*, superimposition of the NAMPT$_2$-GAPDH *cartoon* onto the SAXS-derived *surface model* (calculated from the *ab initio* DAMFILT model and shown in *gray*). *Right*, scattering curves calculated on the model (*green*) compared with the experimental curve (*red*, shown in the *inset*) and the *table* indicating the forward scattering intensities, radii of gyration, and maximal particle dimensions determined from Guinier analysis and the pair distribution function.

binant enzymes confirmed the interaction, both by Western blotting and by silver staining (Fig. S1*a*). A single-cycle surface plasmon resonance (SPR) kinetics experiment was then carried out, in which the His-tagged NAMPT protein was captured as ligand via an anti-His antibody, and GAPDH was injected as analyte at five different concentrations (*i.e.* 0.12–10 μM). The resulting sensorgram after double-referencing, subtraction of signal from Fc1, reference surface, and "zero sample concentration" control cycle, was fitted according to a 1:1 binding mode and, despite the low signal in terms of resonance units, gave a K_D value of 9.7 nM (Fig. 2*a*). The reliability of the kinetic constants calculated by assuming a 1:1 binding model is supported by the quality assessment indicator values, χ^2 of 0.358 and *U*-value of 12. To confirm this, we performed a multiple-cycle kinetic SPR experiment using GAPDH as bait, directly immobilized onto a sensor chip via amine coupling, and NAMPT as analyte in a concentration range closer to the K_D value calculated in the previous experimental session (1–100 nM). The calculated K_D of 7.8 nM was superimposable to the previous SPR analysis (Fig. 2*b*).

These data confirm that NAMPT and GAPDH interact in cells, that this interaction is direct, and that the two proteins show high affinity for the complex.

The complex assembly corresponds to a heterotrimeric NAMPT$_2$-GAPDH oligomer

In the cytosol, NAMPT is a functional dimer (22), and GAPDH is usually a homotetramer (23). However, GAPDH has been shown to have different oligomeric states according to the functions it exerts. For example, it regulates the cytoskeletal dynamics in the cytosol by interacting with actin and tubulin as a monomer (24), it associates with voltage-dependent anion channel 1 (VDAC1) in the mitochondria in the dimeric or tetrameric conformation (21), and it is found in the nucleus as a monomer (25). To understand the oligomeric assembly of the complex, we used pure and homogeneous preparations of both enzymes in size-exclusion chromatography (SEC) co-fractionation experiments. SDS-PAGE analysis of the SEC fractions showed that the two proteins co-elute from the column in a single broad peak, at an elution volume that corresponds to a 140-kDa molecular mass and a Stokes radius (R_S) of 41.8 Å (Fig. 2*c*). This molecular weight, which is not compatible with NAMPT$_2$-GAPDH$_4$, indicates a different oligomeric rearrangement.

We next performed small-angle X-ray scattering (SAXS) experiments on the NAMPT-GAPDH complex in solution. To this end, we measured the scattering from the complex by

Table 1

Kinetics parameters for the reaction of NAMPT, NAMPT5X, and GAPDH in their free form and in NAMPT$_2$::GAPDH complex, at the indicated concentration, respectively

All experiments were performed in triplicate. All data are expressed as the mean ± S.D.

	K_m	V_{max}	K_{cat}
	μM	*nmol/min*	min^{-1}
NAMPT*wt*	4.47 ± 0.80	0.164 ± 0.01	117.14
NAMPT*5xMut*	4.77 ± 0.81	0.198 ± 0.006	141.42
NAMPT*wt*::GAPDH	6.87 ± 0.58	0.163 ± 0.009	116.42
NAMPT*5xMut*::GAPDH	5.26 ± 0.77	0.169 ± 0.008	120.71
GAPDH	118 ± 30	0.031 ± 3.4e − 3	126.80
GAPDH::NAMPT*wt*	78 ± 11	0.018 ± 9.9e − 4	72.40
GAPDH::NAMPT*5xMut*	67 ± 18	0.029 ± 2.7e − 3	116.00

recording 10 exposures of 1 s each on the sample concentrated at 1.15 mg/ml. The comparison of the 10 scattering curves of each sample did not reveal radiation-induced damage, and all of the traces juxtaposed with no outliers. The Guinier plot and the correspondent residual analysis in the Guinier region 1 (Fig. S1*b*) revealed that the preparations were not affected by aggregation phenomena and/or interparticle interference. The analysis of the pair distribution curve highlighted that the ratio between the R_g, calculated by SAXS (33.6 Å) and the R_S, calculated by SEC (41.8 Å), corresponded to 0.80, indicating that the complex adopts a globular shape in solution ($R_g/R_S < 1$). The shape did not superimpose to the shape of the two single proteins alone (data not shown), whereas it resembled a dimer of NAMPT and a monomeric unit of GAPDH (NAMPT$_2$-GAPDH), in full accord with the weight estimated in SEC.

Having ascertained the stoichiometric ratio, we then investigated whether the activity of the two enzymes recruited in the complex varied. As described in Table 1, we did not detect any significant difference in the kinetic parameters of NAMPT in the presence or absence of GAPDH, in accord with the fact that NAMPT remains a dimer. When GAPDH activity was assessed, instead, we observed a reduction in the catalytic efficiency, which might be attributable to the change in oligomerization (Table 1 and Fig. S9).

Identification of the binding interface between NAMPT$_2$-GAPDH complex

We next modeled the organization of the complex to identify the interface by using the homodimeric structure of NAMPT (Protein Data Bank (PDB) code 5U2M) (22) and the monomeric structure of GAPDH (PDB code 5C7I) (23). The docking simulation was performed using the Haddock web server (26). Because we had no information about the regions or amino acids of either NAMPT or GAPDH directly involved in the formation of the complex, we used the C-Port predictor (27) to obtain a well-defined group of residues to drive the Haddock runs. The different NAMPT$_2$-GAPDH complexes obtained through the docking approach were ranked based on the Haddock score, which represents a binding free energy–like value (see supporting information). The three-dimensional structure of the complex with the best haddock score was selected for further analyses (Fig. 2*d*). The ATSAS software demonstrated good agreement, with a χ of 5.93, between the modeled complex and the experimental data comprising the scattering curve and the R_g value determined by SAXS (Fig. 2*d* and Fig. S1*b*). In the modeled complex, GAPDH lies at the level of the interface between the two monomers of NAMPT, establishing a significant number of contacts mainly involving a poorly structured region composed of flexible loops exposed on the surface of the protein. More specifically, as shown in Fig. 3*a*, the monomer A of NAMPT participates in the complex with three different regions: Glu^{38}–Gly^{61} (*red*), Lys^{389}–Lys^{400} (*cyan*) and Phe^{414}–Arg^{429} (*magenta*). The loop between residues Ser^{382} and Leu^{395} (*yellow*) of monomer B stabilizes the crave forming the binding region. Interestingly, the Glu^{38}–Gly^{61} region includes a structurally unresolved loop of NAMPT, whose function has recently been investigated (28) and in which the stretch from amino acid 42 to 51 contributes to the nicotinamide binding. We therefore decided to evaluate the effect of nicotinamide, alongside glyceraldehyde 3-phosphate (G3P), NMN, and NADH, on the stability of the complex. Whereas NMN or NADH had a weak effect on the complex, both nicotinamide and G3P seemed to positively contribute to the complex formation (Fig. S1*c*). This might be the consequence of the fact that dynamic and unstructured loops are characterized by high flexibility in the ligand-free conformation, whereas the ligand-bound form undergoes less prominent structural changes (29).

We then tested the model by designing interfering peptides based on the GAPDH residues that are putatively located at the binding interface. Peptide G1 was designed based on a broad loop between Ala^{178} and Ile^{204}. More specifically, it is constructed joining noncontiguous sequences predicted to be at the interface (TVDGDWRGGRG; *zoom-in* in Fig. 3*a*, *green loop*). SPR analysis showed that G1 bound His-NAMPT with a K_D value of 21.6 μM, showing a biphasic binding behavior during the association step (Fig. 3*b*). Despite the low affinity, G1 allowed us to sustain the reliability of our complex model. In order to validate the G1 peptide, we analyzed the complex preincubated with G1 in SEC. The elution profile showed the presence of two distinct peaks, indicating that G1 was able to perturb the complex (Fig. 3*c*). We also attempted to use a peptide that encompassed positions His^{201}–Ala^{211} (G2 = HQNIIPSSTGA) or extending the regions of interface of G1 (G3 = TVDGPSKKDWRGGRGAHQNI; G4 = TVDGDWRGGRGAHQNIIPSSTGA), but these latter peptides showed lower affinities ($K_D > 500$ μM).

In parallel, we cross-linked recombinant His-NAMPT and GAPDH with disuccinimidyl suberate, alone or in complex at different ratios, and we ran the samples on SDS-polyacrylamide gels. We observed the formation of different oligomeric states of the proteins, and we selected the bands corresponding to 120–160 kDa on the basis of previous size-exclusion chromatography (Fig. S1*d*). We digested them with trypsin prior to cross-linked (XL) LC-MS/MS analysis to identify the putative cross-linked interfaces. We were able to identify nine cross-linked NAMPT and GAPDH peptides that validated the docking model (Fig. 3*d* and Fig. S1*e*). Interestingly, one cross-linked interface between NAMPT and GAPDH, *highlighted* in *red* in Fig. 3*d*, is located in the same amino acid zone used to synthetize the G1 peptide.

To validate the disposition of NAMPT in our model, we decided to investigate two mutants of NAMPT: 2xMut NAMPT, in which Lys^{42} and Lys^{48} were substituted with an

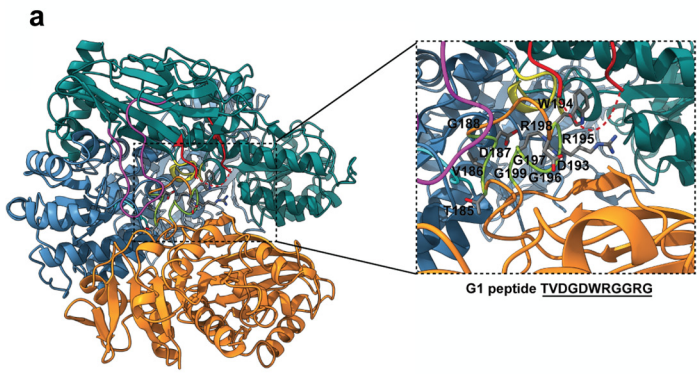

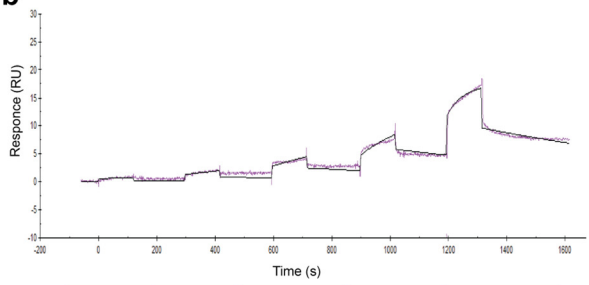

SPR analysis	K_D (μM)	Rmax (RU)	Chi²(RU²)	U-value
	21.6	11.1	0.64	7

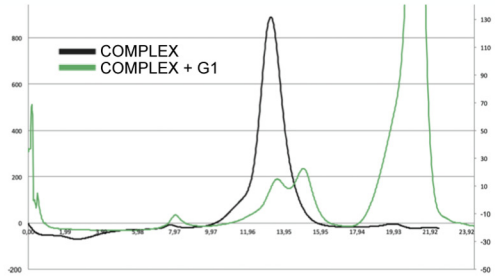

d

Cross-linking LC-MS data			
XL Peptides list		XL K residues list	
NAMPT	GAPDH	NAMPT	GAPDH
TENSKVR(5)	LEKPAKYDDIK(3)	K48	K249
GKVVTK(2)	LEKPAKYDDIK(3)	K73	K249
IQEAKEVYR(5)	PAKYDDIK(3)	K84	K252
KFPVTENSK(1)	TVDGPSGKLWR(8)	K331	K192
DPVADPNKR(8)	YDDIKK(5)	K423	K257
NGKVTK(3)	LEKPAK(3)	K466	K249
VTKSYSFDEVRK(3)	AGAHLKGGAKR(6)	K469	K111
VTKSYSFDEVR(3)	PAKYDDIK(3)	K469	K252
VTKSYSFDEVRK(3)	VVDLMAYMASKE(11)	K469	K332

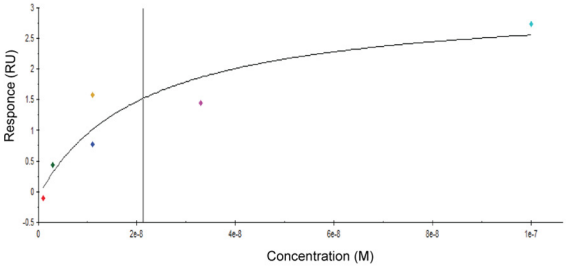

SPR analysis	K_D (nM)	Rmax (RU)	Chi²(RU²)	Offset (RU)
	21.2	3.19	0.211	0.0762

Figure 3. Identification of binding interface between NAMPT and GAPDH. *a*, highlighted loops of the binding interface in the docking model of the complex. Monomer A of NAMPT participates in NAMPT$_2$-GAPDH with three different regions: Glu^{38}–Gly^{61} (*red*), Lys^{389}–Lys^{400} (*cyan*), and Phe^{414}–Arg^{429} (*magenta*). Monomer B of NAMPT participates with the loop between residues Ser^{382} and Leu^{395} (*yellow*). *b*, SPR-based single-cycle kinetics analysis of the interaction between NAMPT, immobilized onto a CM5 chip through an anti-His antibody, and the peptide G1. The G1 peptide was tested at five different concentrations from 300 μM to 3.7 μM. *c*, SEC analysis of the complex alone (*black*) or the complex preincubated for 30 min at 4 °C with 1 mM G1. *d*, XL peptide list obtained by XL LC-MS/MS analysis of cross-linked recombinant NAMPT and GAPDH. The *red* peptide corresponds to the G1 zone. *e*, steady-state affinity analysis of SPR-based multiple-cycle kinetics of GAPDH-NAMPT interaction. 1.2, 3.7, 11, 33, and 100 nM 5xMut NAMPT solutions were injected onto a CM5 chip coated with GAPDH protein immobilized through amine coupling.

alanine, and 5xMut NAMPT characterized by the following site-directed mutagenesis: K42A, K43A, K48A, K51A, and R50A. Indeed, XL LC-MS/MS analysis and our model showed that Lys^{48} of NAMPT is a crucial residue for NAMPT$_2$-GAPDH binding. As shown in Fig. 3*a*, it is located on the surface loop, represented in *red*, and interacts with the residues present on the GAPDH surface loop (*green*). In addition, Lys^{48} is located far from the catalytic site and might not be involved in the enzymatic activity. The other residues were chosen as they are located in the same loop in proximity to Lys^{48}. SEC analysis showed that both 2xMut NAMPT and 5xMut NAMPT eluted at an exclusion volume comparable with that calculated for the WT protein, showing that the point mutations did not affect the dimeric quaternary structure (Fig. S2*a*). In addition, these two NAMPT mutants retained the same enzymatic activity of the WT form (Fig. S2*b* and Table 1). When recombinant GST-GAPDH was immobilized on GST-resin and incubated with His-NAMPT (WT or mutated), both 2xMut NAMPT and 5xMut NAMPT showed a lower ability to bind to GAPDH. In particular, the 5xMut NAMPT showed the lower response in terms of binding to GAPDH in the pulldown experiments (Fig. S2*c*). In good agreement, SEC-based analysis revealed that 5xMut NAMPT shows lower capability to form a stable complex with GAPDH (Fig. S2*d*). Last, 5xMut NAMPT was characterized by a 3-fold lower affinity toward GAPDH with a K_D of interaction of 21.2 nM, as determined by SPR (Fig. 3*e*). In the

presence of GAPDH, the kinetic parameters of NAMPT 5xMut were unchanged, as for WT. As expected, all of the kinetic parameters of GAPDH, in the presence of NAMPT 5xMut, were similar to those obtained with free GAPDH, unlike what was observed in the presence of WT NAMPT (Table 1). This identified area therefore represents the binding zone for interaction between GAPDH and NAMPT to form a NAMPT$_2$-GAPDH complex.

NAMPT and GAPDH are also localized in the nucleus, and their nuclear levels are modulated in stress conditions

Although both GAPDH and NAMPT are primarily localized in the cytosol, we have previously found that in melanoma specimens, we could detect a strong nuclear staining for NAMPT (30). We therefore decided to investigate whether this nuclear localization was maintained in B16 cells and whether GAPDH showed a similar pattern. In both immunocytochemistry and fractionation analysis (Fig. S3), NAMPT and GAPDH displayed a predominant cytosolic localization, but there was a significant presence of both proteins in the nucleus of B16 cells. We performed the same fractionation analysis on a number of other cancer cell lines (*i.e.* 4T1, MSTO, U2OS, HCT116, U87, SH-SY5Y, and HeLa cells), and in most of these, we found that GAPDH and NAMPT were also located in the nucleus, albeit in different levels and proportions (Fig. S3*a*). We also evaluated NIH3T3 cells, in which basal NAMPT and GAPDH expression levels were similar to those of B16 cells (Fig. S3*b*). In these cells, the complex was barely detectable (Fig. S3*b*), as was the nuclear localization of both proteins (Fig. S3, *c* and *d*). This suggests that the subcellular localization of the proteins might influence the complex formation.

We next decided to modulate the protein levels in the nucleus by inducing cellular stress, as reported in the literature for GAPDH (34). We treated B16 cells with H_2O_2 (750 μM) or with *S*-nitrosoglutathione (GSNO; 750 μM) and evaluated cytosol and nucleus fractions after 4 or 24 h. After 4 h, a reduction of both GAPDH and NAMPT was observed in the nucleus. However, after 24 h of treatment, both NAMPT and GAPDH significantly increased in the nucleus compared with control untreated cells (Fig. 4, *a* and *b*). Neither 24 nor 4 h of stress caused an appreciable change in protein amounts of NAMPT or GAPDH in the cytosol of B16 cells (Fig. S4). On the contrary, we failed to observe NAMPT and GAPDH movements at 4 h in NIH3T3 cells (Fig. 4, *a* and *b*), whereas 24-h exposure to any of the two stressors led to cell death (data not shown).

We next evaluated whether direct DNA damage induced by UV or by alkylating agents was also able to attract GAPDH and NAMPT to the nucleus. As shown in Fig. 4 (*c* and *d*), UV radiation, etoposide, or cisplatin induced a significant increase in nuclear NAMPT and nuclear GAPDH after 3 h of recovery from DNA damage. This evidence was confirmed by fluorescence microscopy in GFP-NAMPT and RFP-GAPDH co-expressing cells, which showed augmented movements to the nucleus following etoposide treatment (Fig. 4*e*). Overall, these data show that alongside GAPDH, which had been previously reported (21), also NAMPT may modify localization in response to stressors and that the two proteins appear to shuttle together.

The NAMPT$_2$-GAPDH complex is required for nuclear shuttling

GAPDH has been reported to act as a relay molecule between cellular compartments during cellular stress (31–33), and we therefore investigated whether the complex was involved in the cytosol-to-nucleus translocation. First, we generated B16 stable cell lines silencing 82 ± 1% of NAMPT (shNAMPT) or 61 ± 4% of GAPDH (shGAPDH). Silencing of GAPDH did not affect expression of total or cytosolic NAMPT and vice versa (Fig. 5 (*a* and *b*) and Fig. S5)). Importantly, in shGAPDH cells, the levels of nuclear NAMPT were significantly reduced compared with WT cells, whereas there was a trend in reduction in nuclear GAPDH in shNAMPT cells, although this was not statistically significant (Fig. 5, *a* and *b*). In this context, it has been previously shown that GAPDH translocates to the nucleus via Siah1 in response to stress (34). We therefore decided to investigate whether omigapil, a specific inhibitor of the Siah1-GAPDH interaction (35), could impede nuclear translocation of both NAMPT and GAPDH under DNA damage. Omigapil pretreatment did not affect total cellular levels of NAMPT or GAPDH (Fig. S5*b*), whereas it significantly reduced the translocation of both proteins to the nucleus triggered by UV radiation (Fig. 5, *c* and *d*). The same results were observed in B16 shNAMPT cells (Fig. 5, *c* and *d*). In shGAPDH cells, the nuclear increase was instead compromised for both proteins (Fig. 5, *c* and *d*). Taken together, our data suggest that the reduction of GAPDH expression or the inhibition of GAPDH translocation affects nuclear NAMPT transport after DNA damage.

To specifically interfere with NAMPT$_2$-GAPDH complex, we investigated whether G1 could be used by joining it to a cell-permeant Tat sequence, but unfortunately this peptide lost 40-fold affinity as determined by SPR (K_D ~800 μM). To overcome this limitation, we generated stably expressing B16 WT GFP-NAMPT (*WT*) or 5xMut GFP-NAMPT (*5xMut*) cells, which expressed similar levels of total NAMPT (Fig. S6). The immunoprecipitation conducted with GFP-trap confirmed the data obtained with the recombinant proteins (Fig. 3*e* and Fig. S2), in which the mutant was less able to bind to GAPDH compared with WT (Fig. 5*e*). Importantly, 5xMut GFP-NAMPT was significantly reduced in the nucleus compared with the WT GFP-NAMPT (Fig. 5, *f* and *g*). In addition, immunoprecipitation with GFP-beads demonstrated that both forms of GFP-NAMPT (WT and 5xMut-NAMPT) were able to bind the endogenous NAMPT to form the functional dimer (Fig. 5*e*). For this reason, we observed also a significant reduction of endogenous NAMPT into the nucleus in B16 5xMut GFP-NAMPT cells. More importantly, the levels of nuclear GAPDH were significantly reduced in B16 5xMut GFP-NAMPT cells (Fig. 5, *f* and *g*), both when determined by Western blotting and immunofluorescence.

To confirm the presence of the NAMPT$_2$-GAPDH complex also in the nucleus, we capitalized on a previous report that GAPDH resides on chromatin (36). After acidic extraction of histones in B16 cells, we found that both NAMPT and GAPDH were present on chromatin. We then used the chromatin extract to immunoprecipitate NAMPT with a αNAMPT, and we observed that GAPDH was present as an interactor, as shown in Fig. 5*h*. Moreover, UV radiation, etoposide, cisplatin,

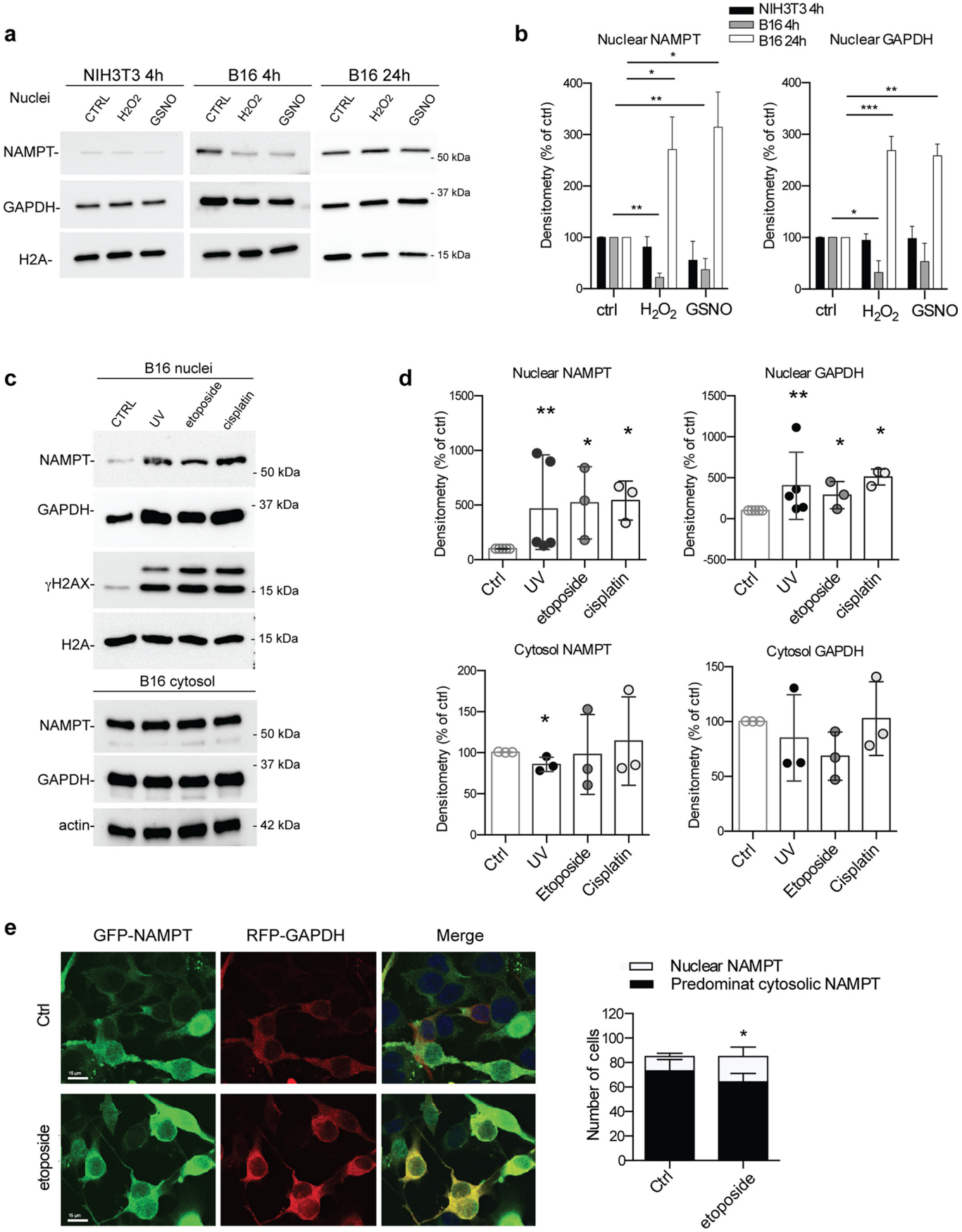
a
NIH3T3 4h
B16 4h
B16 24h
Nuclei
CTRL
H2O2
GSNO
NAMPT-
GAPDH-
H2A-
50 kDa
37 kDa
15 kDa
b
NIH3T3 4h
B16 4h
B16 24h
Nuclear NAMPT
Nuclear GAPDH
Densitometry (% of ctrl)
ctrl
H2O2
GSNO
c
B16 nuclei
CTRL
UV
etoposide
cisplatin
NAMPT-
GAPDH-
γH2AX-
H2A-
50 kDa
37 kDa
15 kDa
B16 cytosol
actin-
42 kDa
d
Nuclear NAMPT
Nuclear GAPDH
Cytosol NAMPT
Cytosol GAPDH
Densitometry (% of ctrl)
Ctrl
UV
etoposide
cisplatin
Etoposide
Cisplatin
e
GFP-NAMPT
RFP-GAPDH
Merge
Ctrl
etoposide
Nuclear NAMPT
Predominat cytosolic NAMPT
Number of cells

and dacarbazine all increased NAMPT and GAPDH on chromatin (Fig. 5*i*). This also occurred in U2OS cells, a classical cell line used for DNA damage investigations, but not in NIH3T3 (Fig. S7).

NAMPT$_2$-GAPDH contributes to fill the nuclear NAD pool

NMNAT1 is localized and active inside the nucleus, but how its substrate, NMN, is available at this level is not completely clear (37). We therefore reasoned that it would be plausible that GAPDH brings NAMPT to the nucleus to increase NMN/NAD$^+$ levels. To demonstrate this, we measured the nucleotide amount extracted from both cytosol and nuclei through a highly sensitive HPLC method based on derivatization with acetophenone and spectrofluorometric quantification. After etoposide exposure, we observed an increase in NMN levels in the nucleus concomitantly to NAMPT translocation. Importantly, pretreatment with omigapil reduced NMN levels (Fig. 6*a*). Furthermore, modulation of NMN levels was correlated with NAMPT movements after oxidative stress induction (Fig. 4*a*), showing lower levels compared with control at 4 h, which increased after 24 h (Fig. 6*a*). This increase in nuclear NMN was directly correlated with nuclear NAD$^+$ (Fig. 6*b*). Importantly, in the cytosol, we did not observe any significant change in both NMN and NAD$^+$ levels (Fig. S8*a*).

To further demonstrate that the amount of NMN in the nucleus was strictly linked with GAPDH-mediated shuttling of NAMPT, we measured the nucleotide levels in GAPDH-silenced cells. As expected, we observed that in B16 shGAPDH melanoma cells, the nuclear pool of NMN, unlike the cytosolic one (Fig. S8*b*), was significantly reduced (Fig. 6*c*).

To determine the absolute NAD$^+$ levels in the nucleus, we made use of a recently described circularly permutated Venus (cpVenus)-based NAD$^+$ biosensor adapted to be localized in the nucleus (38), and we expressed it in A375 human melanoma cells (Fig. 6*h*). After calibration (39), we found that basal nuclear NAD$^+$ was ~260 μM. This level rose by about 40% after UV damage or after 24-h treatment with reactive oxygen species (*ROS*; Fig. 6*i*). In analogy to the localization of NAMPT and GAPDH, which were reduced after 4 h of treatment, NAD$^+$ levels dropped at this time (Fig. 6*i*).

Last, to conclusively demonstrate that NMN and NAD$^+$ levels in the nucleus were dependent on NAMPT movements, we engineered a NAMPT with the nuclear localization sequence of SV40 at the N terminus linked to a FLAG tag to specifically recognize it (NLS-NAMPT) and expressed it in HEK293T cells, which have low basal NAMPT-GAPDH interaction (Fig. 1) and a faint NAMPT nuclear localization (Fig. S8*c*). This resulted in a stable line of cells that expressed NLS-NAMPT exclusively in the nucleus (Fig. S8*d*). An increase in both NMN levels (Fig. 6*d*) and NAD$^+$ levels (Fig. 6*e*) in the nucleus of these cells was observable. Finally, we confirmed that the 5xMut GFP-NAMPT cells also expressed less NMN and NAD$^+$ in the nucleus (Fig. 6, *f* and *g*). Last, we performed preliminary experiments to evaluate the biological consequences of the lack of NAMPT$_2$-GAPDH complex formation and whether B16 5xMut GFP-NAMPT cells duplicate differently from B16 WT GFP-NAMPT cells. We did not observe a difference in the growth rate of the two cell lines in basal conditions (Fig. 5*j*), whereas we observed that 5xMut NAMPT conferred a small, albeit significant, increased sensitivity to etoposide (Fig. 5*k*).

Discussion

NMNAT isoforms are distributed in the cytosol, nucleus, and mitochondria, whereas NAMPT is localized in the cytosol (15, 40). Although it is plausible that NMN can diffuse across the nuclear envelope, it would appear counterintuitive to segregate the two enzymes. Indeed, in a recent work, Kraus and collaborators (37) postulate that NMN could be a common substrate for both cytosolic and nuclear transferases, possibly suggesting that NMN is freely diffusible. However, given the presence of nuclear NAD-consuming enzymes (*e.g.* PARPs and sirtuins), it would appear more efficacious to have the entire salvage pathway located in the nucleus. Indeed, the maintained nuclear localization of NMNAT1 during evolution suggests that *in loco* synthesis is important.

In the present work, we provide evidence that NAMPT translocates to the nucleus when NAD$^+$ replenishment is required. In particular, we demonstrate that NAMPT interacts with GAPDH to form a complex in the cytosol and that the NAMPT$_2$-GAPDH complex translocates to the nucleus. We also establish that NAMPT, in the nucleus, contributes to replenishment of the NMN/NAD pool.

To demonstrate that NAMPT and GAPDH stably interact, we have shown that these two proteins immunoprecipitate together in cells and that a specific NAMPT inhibitor (UG1006), immobilized on specific resin, is able to pull down both NAMPT and GAPDH. In addition, we have shown that recombinant proteins form a direct complex via pulldown experiments; the affinity of the proteins for the complex is in the nanomolar range, and we demonstrate that the complex is present also in the nuclear compartment, bound to chromatin. Finally, we validated the NAMPT_GAPDH complex arrangement (dimer of NAMPT and monomer of GAPDH) with SAXS experiments, SEC analysis, and XL-LC-MS analysis. This arrangement was further strengthened by kinetic analysis, in which NAMPT did not change its kinetic parameters when in the NAMPT$_2$-GAPDH complex (as it remained a dimer), whereas GAPDH in the presence of WT NAMPT lost efficiency

Figure 4. Nuclear levels of NAMPT and GAPDH are modulated by stress conditions in B16 melanoma cells. *a*, representative Western blotting of nuclear fractions of NIH3T3 and B16 cells treated with 750 μM H_2O_2 and 750 μM GSNO for 4 or 24 h. *b*, densitometry of Western blot analysis of nuclear fractions of NIH3T3 treated with H_2O_2 and GSNO for 4 h ($n = 3$ independent experiments) and B16 treated for 4 and 24 h ($n = 3$ independent experiments). *c*, representative Western blotting of nuclear (*top*) and cytosolic (*bottom*) fractions of B16 melanoma cells. Cells were treated once with UV radiation (20 s) or 10 μM etoposide (1 h) or 20 μM cisplatin (1 h). Fractionation was conducted after 3 h of recovery since induced DNA damage. *d*, densitometry of Western blot analysis of nuclear fractions of B16 cells treated with UV ($n = 5$ independent experiments) or with etoposide or cisplatin ($n = 3$ independent experiments) and densitometry of Western blot analysis of cytosolic fractions ($n = 3$ independent experiments). *e*, B16 melanoma cells were stably infected with lentiviral vectors expressing GFP-NAMPT and RFP-GAPDH and treated with 5 μM etoposide for 1 h. Nuclei were stained with DRQ5. Cells were analyzed by a confocal microscope, and nucleus-positive cells were counted ($n = 510$ cells, mean of 80 cells/field). Statistical analysis was by a two-tailed, unpaired Student's *t* test. Data are presented as the means ± S.E. (*error bars*). *, $p < 0.05$; **, $p < 0.01$; ***, $p < 0.001$.

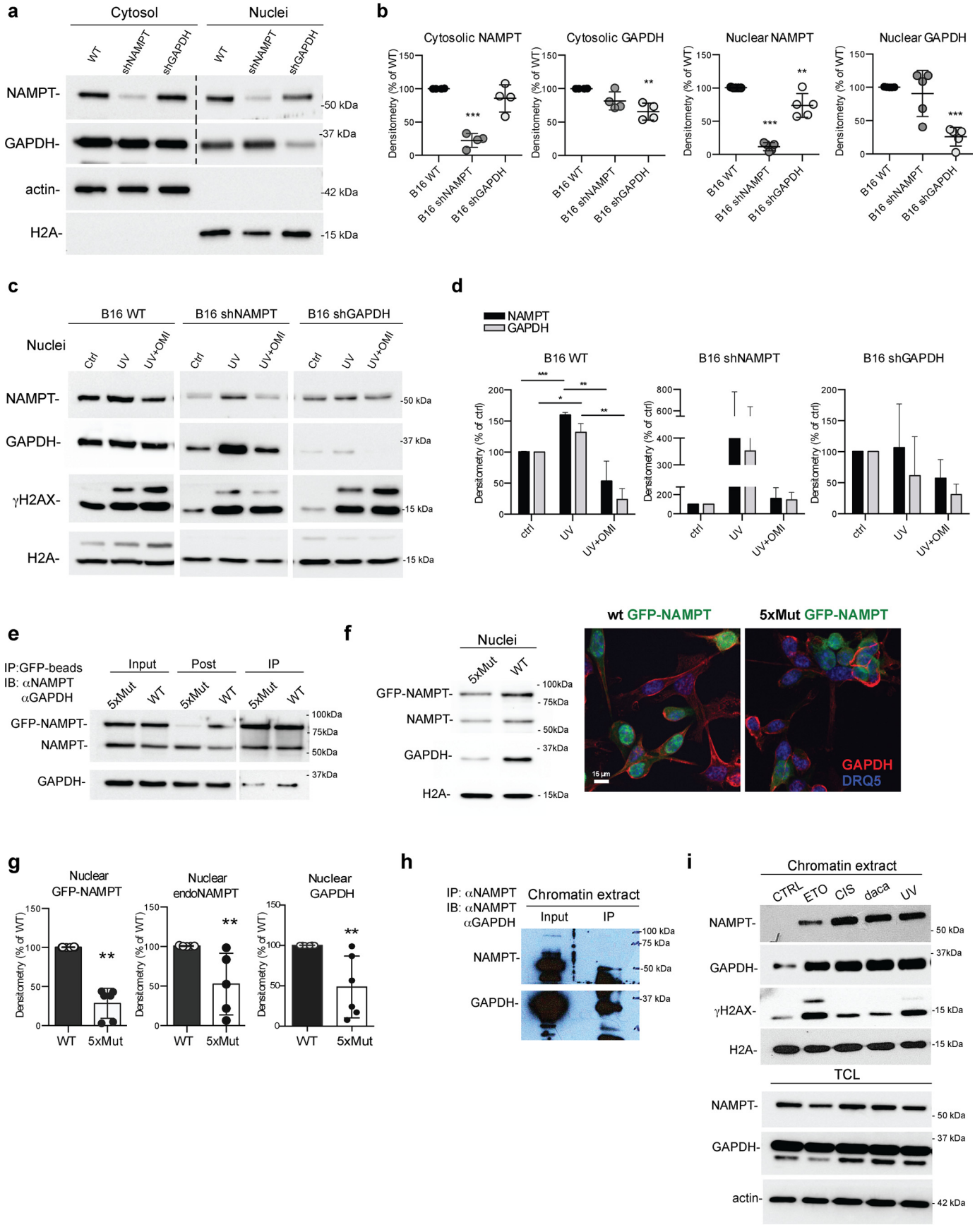
a
Cytosol
Nuclei
WT
shNAMPT
shGAPDH
NAMPT-
GAPDH-
actin-
H2A-
-50 kDa
-37 kDa
-42 kDa
-15 kDa
b
Cytosolic NAMPT
Cytosolic GAPDH
Nuclear NAMPT
Nuclear GAPDH
Densitometry (% of WT)
B16 WT
B16 shNAMPT
B16 shGAPDH
c
B16 WT
B16 shNAMPT
B16 shGAPDH
Nuclei
Ctrl
UV
UV+OMI
NAMPT-
GAPDH-
γH2AX-
H2A-
d
NAMPT
GAPDH
Densitometry (% of ctrl)
ctrl
UV
UV+OMI
e
IP:GFP-beads
IB: αNAMPT
αGAPDH
Input
Post
IP
5xMut
WT
GFP-NAMPT-
NAMPT-
GAPDH-
f
Nuclei
wt GFP-NAMPT
5xMut GFP-NAMPT
GFP-NAMPT-
NAMPT-
GAPDH-
H2A-
GAPDH
DRQ5
15 μm
g
Nuclear GFP-NAMPT
Nuclear endoNAMPT
Nuclear GAPDH
Densitometry (% of WT)
WT
5xMut
h
IP: αNAMPT
IB: αNAMPT
αGAPDH
Chromatin extract
Input
IP
NAMPT-
GAPDH-
i
Chromatin extract
CTRL
ETO
CIS
daca
UV
NAMPT-
GAPDH-
γH2AX-
H2A-
TCL
actin-

as a monomer. SAXS experiments, SEC analysis, and XL-LC-MS analysis have also allowed us to determine the area of interaction of the two proteins, which does not impinge on the enzymatic activity of the single proteins. A low-affinity interfering peptide designed on the area of interaction (G1) allowed us to disrupt the complex, providing conclusive evidence.

To demonstrate that the $NAMPT_2$-GAPDH complex is required to allow entry to the nucleus of NAMPT, we have shown that stressful stimuli that are known to consume nuclear NAD^+ (oxidative stress, NO-induced stress, DNA damage) lead to the movement of both proteins to the nucleus, as seen in immunocytochemistry, fluorescence microscopy, and fractionation experiments. Moreover, we have shown that reducing the levels of GAPDH via shRNA reduces the amount of NAMPT that is detected in the nucleus and that omigapil, a drug designed to inhibit GAPDH transport to the nucleus upon stressful stimuli, reduces the translocation of NAMPT to the nucleus. A mutated NAMPT, which displays a lower affinity for GAPDH but identical enzymatic activity, does not translocate as efficiently to the nucleus.

Last, we show that the attraction of NAMPT to the nucleus serves to replenish the NMN/NAD pool, as (i) NMN and NAD^+ levels coincide with the observed translocation of NAMPT, including the treatment with omigapil; (ii) reducing the levels of GAPDH via shRNA reduces the amount of NMN detected in the nucleus but not in the cytosol; (iii) in cells expressing a mutated NAMPT, which shows a lower affinity for GAPDH but identical enzymatic activity, nuclear NAD^+ levels are lower; (iv) tagging NAMPT with an NLS signal increases nuclear NMN/NAD^+ levels; (v) stimuli known to reduce NAD^+ levels via activation of NAD-consuming enzymes increase NAMPT levels in the nucleus. While not contradicting the previous reports that NMN may diffuse to the nucleus (37), therefore, we provide evidence that the presence of NAMPT in the nucleus is able to increase NMN/NAD^+ concentrations above those that would be possible by simple diffusion of the NMNAT1 substrate.

The number of cellular functions that can be attributed to GAPDH is constantly increasing, and indeed it has been referred to as an archetypical moonlighting protein (41). We now demonstrate that control of NAD^+ levels in the nucleus, albeit indirectly, is yet another function that can be ascribed to this protein. While this manuscript was in preparation, another group showed that NAMPT translocates to the nucleus upon stressful stimuli (19). The authors highlight NAMPT residues that might have been responsible for its nuclear movement, and our data are in accordance with their results. In addition, we have identified in NAMPT a superimposable specific region that is fundamental for binding GAPDH to form the $NAMPT_2$-GAPDH complex and that is responsible for its translocation to the nucleus. Svoboda *et al.* (19) predicted that an unidentified "importin" mediated the translocation. Our data suggest that GAPDH should be further investigated, as it might be this importin.

We have detected the $NAMPT_2$-GAPDH complex easily in cancer cells, whereas when investigating noncancerous cells, the complex was more difficult to detect. This may be the consequence of overexpression of these proteins in cancer cells, or it may be the consequence of the need for some post-translational modifications. However, it should be noted that the complex is stable also between recombinant proteins outside the cellular context, thereby suggesting that if there is a specific post-translational modification that increases the chances of stable complex formation in cells, this is not an absolute requirement. In this context, we have found that a number of stimuli (DNA damage inducers and stress inducers) are able to increase nuclear NAMPT and nuclear GAPDH. When evaluating NMN and NAD^+ levels after stimulation, we were also able to find increased nucleotides after 4 h of etoposide treatment, as expected. On the contrary, we were unable to detect increases over control after a 24-h exposure to H_2O_2, although there was a slight recovery from the levels detected after 4 h. This might be due to the difference in stimulus or to a different time course in NAD consumption. Indeed, Svoboda *et al.* (19) have also found a decrease in total NAD^+ after H_2O_2 treatment.

In preliminary experiments, we have found that cells overexpressing 5xMut GFP-NAMPT, which reduces the complex formation, have a small, yet statistically significant, increased sensitivity to etoposide. Whereas this would tend to suggest that the mechanisms described here are protective for cells, better tools need to be engineered to unravel the specific role of the $NAMPT_2$-GAPDH complex in cells. Indeed, despite the biological importance of NAD^+, the physiological role of compartmentalized NAD^+, especially the nuclear NAD^+ biosynthesis, is largely unexplored. In this work, we unravel that NAMPT translocates to the nucleus in a $NAMPT_2$-GAPDH complex upon stress to sustain the NMN/NAD^+ salvage pathway.

Experimental procedures

Cell culture

B16 murine melanoma cells, HeLa human cervical cancer, A375 human melanoma cells, HEK293T human kidney cells,

Figure 5. Nuclear transport of NAMPT depends on GAPDH binding. *a*, representative Western blotting of basal protein levels in cytosolic and nuclear fractions in B16 WT, silencing NAMPT (*shNAMPT*), or silencing GAPDH (*shGAPDH*) cells. In NAMPT and GAPDH blotting, a splice is present between the *cytosol* and *nucleus lanes*. *b*, densitometry of cytosolic and nuclear fractions ($n = 4$ and $n = 5$ independent experiments, respectively). *c*, representative Western blotting of nuclear fractions of B16 WT, shNAMPT, and shGAPDH cells treated for 20 s with UV radiation with or without 30-min pretreatment with 10 μM omigapil (*OMI*). *d*, densitometry of the nuclear fractions. $n = 3$ independent experiments for each cell line. Statistical analysis was by an ordinary one-way analysis of variance, Tukey's multiple-comparison test. *e*, IP conducted with GFP-trap in the cytosol of B16 WT GFP-NAMPT cells (*WT*) or B16 5xMut GFP-NAMPT cells (*5xMut*). Input and Post are shown to compare the two cell lines. *f*, representative Western blotting of nuclear fractions of B16 WT GFP-NAMPT cells (*WT*) or B16 5xMut GFP-NAMPT cells (*5xMut*) and immunofluorescence of WT and 5xMut cells stained for GAPDH (*red*) and nucleus (DRQ5, *blue*). *g*, densitometry of the protein levels in the nuclear fractions of WT and 5xMut cells. $n = 6$ independent experiments. Statistical analysis was by a Mann–Whitney U nonparametric test. Data are presented as the means ± S.E. (*error bars*). *, $p < 0.05$; **, $p < 0.01$. *h*, IP conducted with mouse αNAMPT on chromatin extract from B16 WT cells. *i*, chromatin extract of B16 WT cells treated with 10 μM etoposide, 20 μM cisplatin, 25 μM dacarbazine for 1 h or with 20-s UV radiation. Chromatin extraction was conducted after 3 h of recovery. Total cell lysates (*TCL*) showed no differences in protein expression after the treatments. *IB*, immunoblotting.

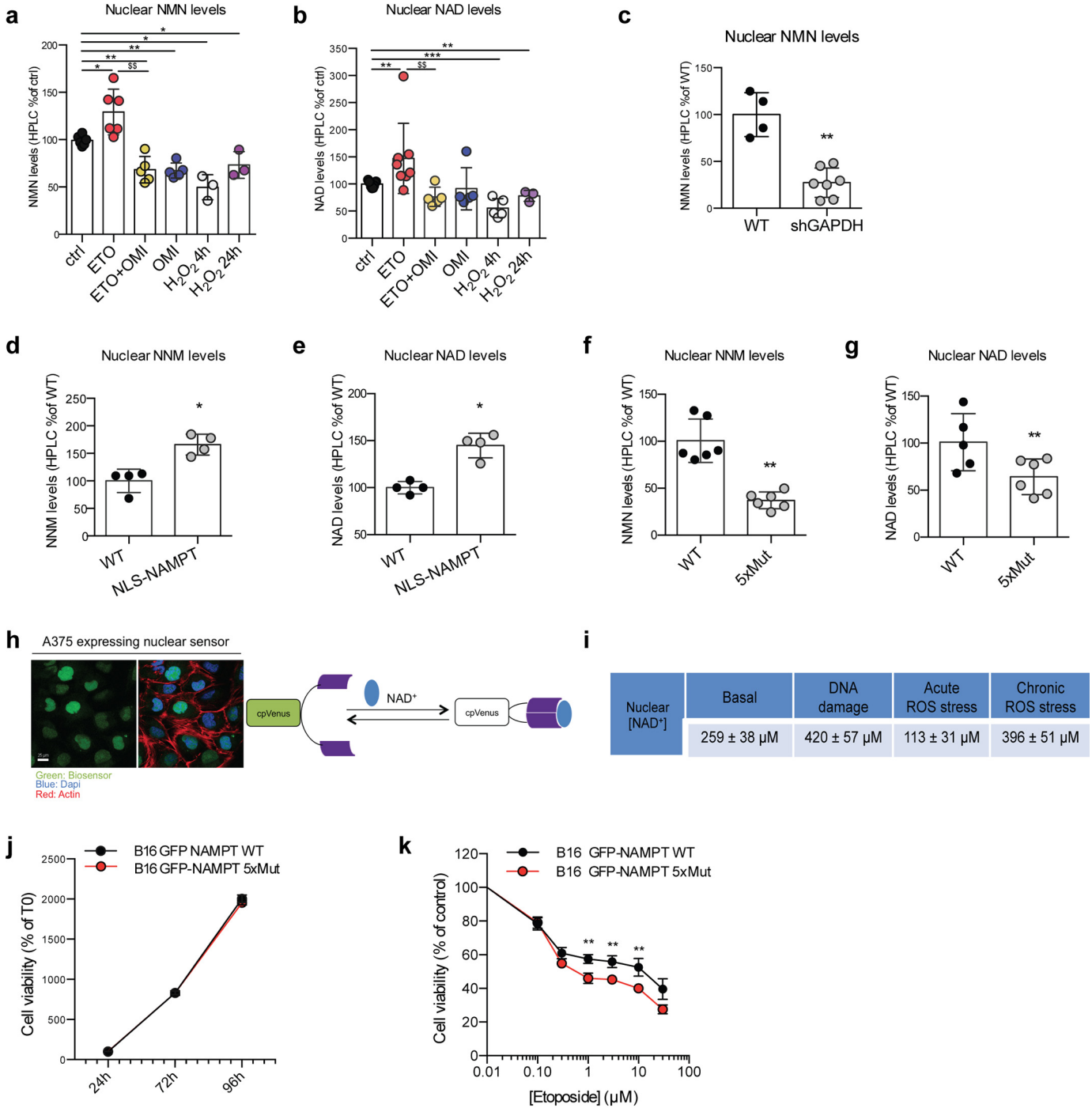

Figure 6. NAMPT transported by GAPDH contributes to fill the NMN/NAD nuclear pool. Nuclear NMN (*a*) and NAD$^+$ (*b*) levels were measured by HPLC after nucleotide acidic extraction. B16 WT cells were treated with 10 μM etoposide (*ETO*) with or without 30-min pretreatment with 10 μM omigapil (*OMI*). After 1 h, cells were replaced with fresh medium, and after an additional 3 h of recovery, cells were fractionated, and nucleotides were extracted ($n = 2$ for three independent experiments). For oxidative stress, cells were incubated for 4 or 24 h with 750 μM H_2O_2 and then fractionated, and nucleotides were extracted ($n = 3$ independent experiments). *c*, nuclei were isolated from B16 WT cells and B16 shGAPDH cells, and nucleotides were extracted and analyzed by HPLC ($n = 4$ independent experiments). Nuclear NMN (*d*) and NAD$^+$ (*e*) levels were measured by HPLC in HEK293T WT cells and overexpressing NLS-NAMPT cells ($n = 4$ independent experiments). Nuclear NMN (*f*) and NAD$^+$ (*g*) levels were measured by HPLC in B16 overexpressing WT GFP-NAMPT (*WT*) or 5xMut GFP-NAMPT (*5xMut*). *h*, confocal image of A375 melanoma cells expressing nuclear cpVenus-based NAD$^+$ biosensor (*left*). *Right*, scheme of the NAD biosensor; when NAD is bound, the fluorescence signal is reduced. *i*, NAD$^+$ concentrations calculated on the basis of a calibration curve through cpVenus-based NAD biosensor in A375 melanoma cells. *j*, cell viability of B16 WT and 5xMut GFP-NAMPT cells at 24–48 and 72 h of growth in basal conditions. *k*, cell viability of B16 cells under a dose-response curve of etoposide. Statistical analysis was by a Mann–Whitney *U* nonparametric test for *a* and *b*. *, *p versus* control; $, *p versus* etoposide. Two-tailed or unpaired Student's *t* test was used for the rest of the graphs. Data are presented as the means ± S.E. (*error bars*). *, $p < 0.05$; **, $p < 0.01$; ***, $p < 0.001$.

and NIH3T3 murine fibroblasts were cultured in Dulbecco's modified Eagle's medium (Sigma–Aldrich). HCT116 human colorectal cancer and U2OS human osteosarcoma were cultured in McCoy's 5a Medium Modified (Sigma–Aldrich). 4T1 murine mammary carcinoma and U87 human glioblastoma were cultured in minimum essential medium Eagle (Sigma–

Aldrich). MSTO human mesothelioma was cultured in RPMI 1640 medium (Sigma–Aldrich). SH-SY5Y human neuroblastoma was cultured in minimum essential medium Eagle + F-12 medium (Sigma–Aldrich).

Media were supplemented with 10% fetal bovine serum (Gibco), 2 mg/ml glutamine, 10 units/ml penicillin, and 100 g/ml streptomycin (Sigma–Aldrich). Human adult melanocytes were provided by ATCC (PCS-200-013), and growth with dermal basal medium supplemented with a melanocyte growth kit (PCS-200-042). Human fetal astrocytes were kindly provided by Eleonora Aronica's laboratory in Amsterdam and cultured in Dulbecco's modified Eagle's medium + F10 medium. Cells were maintained in a controlled atmosphere of 5% CO_2 with humidity at 37 °C. Cells were detached from plates by trypsinization (Sigma–Aldrich).

UG 1006-coupled bead pulldown

Synthesis of UG1006 NAMPT inhibitor and bead conjugation are described in the supporting Methods. We incubated overnight at 4 °C UG1006-beads or control beads with total cell lysates made in radioimmune precipitation assay buffer. Proteins were then eluted from beads through sample buffer incubation, boiled, and analyzed by Western blotting.

Creation of stable infected cell lines

Stable B16 cell lines expressing different constructs were obtained through stable lentiviral infection. Engineered GAPDH or NAMPTs were cloned in the pLV lentiviral vector, RFP-GAPDH, FLAG-NAMPT, WT GFP-NAMPT, or 5xMut GFP-NAMPT, mutated with a site-directed mutagenesis kit from Agilent Technologies according to the manufacturer's instructions by using the following primers: CCTACTTTGAATGCCGTGAAGCGGCGACAGAAAACTCCGCAGTAGCGGCGGTGAAATACGAGGAAAC (forward) and GTTTCCTCGTATTTCACCGCCGCTACTGCGGAGTTTTCTGTCGCCGCTTCACGGCATTCAAAGTAGG (reverse). Correct insertion and sequence of all the plasmids were confirmed by sequencing.

The lentiviral particles were produced as described elsewhere (42) in HEK293T cells transfected with pMDLg/pRRE, pMD2.VSVG, pRSV-Rev, and pLV expressing the protein of interest. Briefly, after 48 h, cell medium was collected, filtrated, and centrifuged for 2 h at 70,000 × *g*. The viral particles, corresponding to the pellet fraction, were resuspended and used to infect B16 cells, after virus titration. Expression was monitored by Western blot analysis or FACS analysis. When necessary, cells were flow-sorted for high positive fluorescence (S3e Cell Sorter, Bio-Rad).

B16 shNAMPT and shGAPDH cell lines

The lentiviral particles were produced as described above in HEK293T cells by a second-generation packaging plasmid system added with GIPZ mouse NAMPT lentiviral shRNA plasmid (ID: V3LMM_518294) (GE-Dharmacon) or GIPZ Mouse GAPDH lentiviral shRNA plasmid (ID: V2LMM_159063) (GE-Dharmacon). The viral particles were used to infect B16 cells, and a stable cell line was created. The infected cells were sorted for high levels of GFP. Silencing was confirmed by Western blot analysis.

HEK293T NLS-NAMPT cells

NLS-NAMPT was obtained by linking at the N terminus of murine FLAG-NAMPT the NLS of SV40 (ATGGCAGTTCCCAAGAAGAAGAGGAAAGTTGAG). The lentiviral vector is a pLV bicistronic vector expressing NLS-FLAG-NAMPT internal ribosome entry site GFP. Cells were stably infected as described above and flow-sorted for GFP$^+$. Expression and localization were analyzed by immunofluorescence and fractionation.

IP

1.0×10^7 cells were lysed in 20 mM HEPES, 100 mM NaCl, 5 mM EDTA, 1% Nonidet P-40 added with protease and phosphatase inhibitor mixture (Millipore). Protein A/G PLUS agarose (Santa Cruz Biotechnology, Inc., sc-2003) were incubated with appropriate antibody (see "Reagents") for 2 h at 4 °C in agitation. Then 500 μg of proteins (apart from the IP in Fig. 1*c*, in which 250 μg were used) were incubated with beads conjugated with the antibody overnight at 4 °C in agitation. Immunoprecipitated proteins were eluted from beads with 0.1 M glycine, pH 2.2, and analyzed by Western blotting. We immunoprecipitated FLAG-NAMPT of GFP-NAMPT using anti-FLAG-M2 affinity gel (A2220, Sigma) or Chromotek GFP-trap agarose (Gta-20), respectively.

Cytosol/nucleus fractionation

1.0×10^7 cells, treated as described in the Figs. 4, 5 and 6 legends, were lysed in a 4× pellet volume of Buffer A (300 mM sucrose, 10 mM HEPES, 10 mM KCl, 2 mM $MgCl_2$, 1 mM EGTA) added with protease and phosphatase inhibitors (Millipore) and with 0.1% of Nonidet P-40 (lysis was controlled by trypan blue). Then cells were centrifuged at 1300 relative centrifugal force for 5 min at 4 °C. Supernatant (impure cytosol) was centrifuged at 13,000 rpm for 15 min to remove the membranes. The pellet (nuclei) was washed five times with Buffer B (50 mM HEPES, 0.4 M NaCl, 1 mM EDTA) and then resuspended in 3× pellet volume of Buffer B added with protease and phosphatase inhibitors, sonicated, and incubated on a thermomixer for 45 min at 4 °C with 1300-rpm rotations every 5 min. Then nuclei were centrifuged for 15 min at 13,000 rpm at 4 °C, and the nuclear proteins resulted into the supernatant. Both cytosols and nuclei were quantified by Bradford reagent (Sigma–Aldrich) and then analyzed by Western blotting.

Western blot analysis

Total cell lysates were obtained by lysing the whole cells in lysis buffer (20 mM HEPES, 100 mM NaCl, 5 mM EDTA, 1% Nonidet P-40) added with protease and phosphatase inhibitor mixture (Millipore). Samples obtained by fractionation were resolved by Western blotting. Protein quantification was performed with Bradford reagent (Sigma–Aldrich), and proteins were resolved on home-made gradient 4–20% SDS-polyacrylamide gels. Densitometry analysis was performed with the Image Lab program (Bio-Rad, Hemel Hempstead, UK). Primary antibodies used are listed under "Reagents." Peroxidase-conju-

gated secondary antibodies were from Bio-Rad. When not transferred onto nitrocellulose, proteins were resolved by silver staining (Pierce kit) or Coomassie staining.

Immunofluorescence

5.0×10^4 cells were fixed in 4% paraformaldehyde on glass coverslips in 24-well plates, permeabilized with 0.1% Triton, and saturated in 0.2% gelatin/PBS. Subsequently, primary antibody (1:100 in 0.2% gelatin) was incubated in a humid chamber overnight at 4 °C. Secondary antibodies (1:500 in 0.2% gelatin) added with DRQ5 (Invitrogen) were incubated for 1 h at room temperature. Fluorescence images were acquired using a Leica (Leica Microsystems, Wetzlar, Germany) epifluorescent microscope equipped with an S Fluor ×40/1.3 numerical aperture objective using METAMORPH (Molecular Devices, Sunnyvale, CA) software.

NMN/NAD$^+$ measurement by HPLC

10×10^6 cells were fractionated to obtain cytosolic and nuclear fractions as described above. Before starting the fractionation, the total protein concentration was calculated. After fractionation, a fixed volume of cytosol was added with one-half volume of 1.2 M $HClO_4$ incubated at 4 °C for 15 min and then centrifuged. Supernatant was collected and added with one-fifth volume of 1 M K_2CO_3. Samples were centrifuged, and the supernatant was analyzed by derivatization with acetophenone, carried out as described (12). On the other hand, the nuclear pellet was resuspended with a 3× volume of 0.4 M $HClO_4$ sonicated and centrifuged. Supernatant was collected and added with one-fifth volume of 1 M K_2CO_3. Samples were centrifuged to eliminate the salt, and the supernatant was analyzed by HPLC to measure NMN and NAD$^+$ levels as indicated above. The above spectrofluorometric C18-HPLC data for acetophenone-derivatized NMN and NAD$^+$ have been referred to mg of proteins that were extracted in parallel from each sample analyzed and then calculated as a percentage of the control.

CpVenus-based NAD$^+$ sensor construct and generation of A375 cells stably expressing nuclear biosensor

The NAD$^+$ biosensor is composed by a cpVenus fluorescent protein linked to a bipartite NAD$^+$-binding domain of a bacterial DNA ligase (LigA1b and LigA1a). Nuclear biosensor expression vector and relative nuclear cpVenus coding construct were kindly provided by X. A. Cambronne (Department of Molecular Biosciences, University of Texas, Austin, TX) (38). The incorporation of specific targeting sequences allows this biosensor to be expressed in a nucleus-specific way. DNA was amplified, incorporated into lentiviral particles, and used for stable cell transduction. Functionally, the LigA-cpVenus biosensor has two excitation peaks, one at 488 nm that decreases according to NAD elevation and a second one at 405 nm that is unaffected by substrate variations, serving as an internal control (38). A375 BRAFV600E-mutated cell lines were from the American Type Culture Collection (ATCC). Cells expressing nuclear biosensor were obtained by transducing A375/sensitive (S) cells with a lentiviral vector carrying the specific organelle-targetable biosensor or with the organelle-targetable cpVenus alone, using polybrene (8 μg/ml; Sigma, Milan, Italy). cpVenus-positive cells were flow-sorted (FACSAriaIII, BD Biosciences, Milan, Italy) and used as reported.

Flow cytometry and statistical analysis

For flow cytometry analysis, cells were trypsinized and collected in RPMI 10% FCS. Sensor/cpVenus FITC (excitation 488 nm, emission 530/30 nm) and BV510 (excitation 405 nm, emission 525/50 nm) were measured by flow cytometry (BD FACS Celesta), and data were processed with DIVA version 8 (BD Biosciences) and FlowJo version 10.01 software (TreeStar, Ashland, OR). Cells were gated using forward scatter and side scatter for the live cells. Doublets were excluded by further gating on both side scatter and forward scatter width, and at least 10^4 cells/sample were analyzed. The statistical analysis required a double ratio (*i.e.* -fold change). The first is the ratiometric 488/405 measurement, detected by the biosensor, and the second is obtained by the parallel analysis of 488-nm/405-nm fluorescence changes of cells expressing the cpVenus-only control (36). The cpVenus 488/405-nm fluorescence *ratio* is used to normalize for NAD changes independent of the biosensor. F0 refers to the double ratio obtained in untreated conditions (F0 = 1). NAD variations are finally expressed as the inverse relationship between the -fold changes and the cofactor concentrations. A -fold change value >1 indicates reduced NAD$^+$ concentrations, whereas values of <1 indicate increased levels of NAD$^+$.

Chromatin extraction

1.0×10^7 cells were harvested in ice and washed with PBS. The pellet was resuspended in ice-cold 5% perchloric acid added with protease inhibitors and incubated for 10 min and centrifuged at 13,000 rpm for 10 min. Supernatant was discarded, and the perchloric acid extraction was repeated twice. Then the pellet was resuspended in a 2× volume of 0.4 N HCl, incubated for 15 min in ice, and centrifuged at 13,000 rpm for 10 min. Supernatant containing histones was harvested. The HCl extraction was repeated three times. All of the supernatants obtained by HCl extraction were collected and precipitated by ice-cold TCA to 25% final concentration to supernatant, incubated for 30 min on ice, and centrifuged at 13,000 rpm for 20 min. The protein pellet was washed with ice-cold 100% acetone, 0.006% HCl and centrifuged at 13,000 rpm for 10 min. The pellet was washed again with 100% acetone and centrifuged as before. Then the protein pellet was dried in a SpeedVac and resuspended in 50 mM Tris-HCl, pH 7.5–8, and protein concentration was quantified by Bradford reagent (Sigma–Aldrich) for Western blot analysis.

Recombinant protein preparation

WT murine full-length NAMPT (ORF GenBank™ BC018358) was cloned in pET28a (NdeI/EcoRI) (43). Murine NAMPT-K(42–48)A and NAMPT-K(42–51)A mutants cloned in pET28a were obtained by using a site-directed mutagenesis kit (Agilent Technologies, Santa Clara, CA) according to the manufacturer's instructions, by using the following primers: CCTACTTTGAATGCCGTGAAGCGGCGACAGAAAACTCCGCAGTAGCGGCGGTGAAATACGAGGAAAC (forward) and GTTTCCTCGTATTTCACCGCC-

GCTACTGCGGAGTTTTCTGTCGCCGCTTCACGGCATTCAAAGTAGG (reverse). cDNA of WT murine full-length GAPDH (murine variant type 2) was derived from B16 melanoma cells and cloned in pET28 (NdeI/XhoI) and in pGEX vector (EcoRI/XhoI). All recombinant proteins were expressed in *Escherichia coli* BL21(DE3) (induction with 0.5 mM isopropyl 1-thio-β-D-galactopyranoside overnight at 20 °C) and purified by tag affinity chromatography with nickel-nitrilotriacetic acid Superflow resin (Qiagen) or with GSH resin (GE Healthcare). The activity of NAMPT proteins was determined by a spectrophotometer continuous assay as described previously paper (44).

Cell viability assay

To analyze cell viability, the colorimetric 3-(4,5-dimethylthiazol-2-yl)-2,5-diphenyltetrazolium bromide (MTT) assay was used. Briefly, cells were plated in 24-well plates and treated as indicated for the appropriate time. Etoposide (dissolved in DMSO) was added at the indicated concentrations. Vehicle control was added to the cells to give a final concentration no greater than 0.1%. MTT (250 μg/ml in Locke buffer) was added, and cells were incubated for 1 h at 37 °C. Then formazan crystals were dissolved in isopropyl alcohol plus 0.1 M HCl. The absorbance was read at 570 nm in a plate reader (Victor3 V, PerkinElmer Life Sciences).

Pulldown assays

To perform the pulldown assay, GAPDH was expressed as a GST fusion protein to be immobilized onto GSH-agarose beads. The chimeric protein contains a cleavage site for the Prescission Protease (GE Healthcare). The immobilization step was performed for 1 h at 4 °C. After washing to remove the unbound protein, the His-NAMPT prey was added to the GST-GAPDH– bound resin or GSH resin (control) in the presence of 50 mM Tris-HCl, 250 mM NaCl, 0.5 mM β-mercaptoethanol, pH 7.5. The binding reaction was performed at 4 °C for 1 h under gentle agitation. Prior to the elution step, the resin was washed five times with 25 ml of the same buffer. Proteins were eluted in 0.5 ml of elution buffer (50 mM Tris-HCl, 150 mM NaCl, 10 mM EDTA, 1 mM DTT, pH 8.0) containing the Prescission Protease, and the eluted samples were then analyzed by Western blotting in the presence of αNAMPT αGAPDH and silver staining.

Size-exclusion chromatography

SEC-based NAMPT-GAPDH co-fractionation experiments were performed using a Superdex 200 10/300 GL column (GE Healthcare), precalibrated with standard proteins (following the manufacturer's instructions), and by fluxing the buffer containing 50 mM Tris-HCl, 250 mM NaCl, 0.5 mM β-mercaptoethanol, pH 7.5, as the mobile phase. All of the chromatographic steps were monitored by 280-nm absorbance reading, and the protein-containing fractions were further analyzed by standard SDS-PAGE analysis.

SAXS

Small-angle X-ray scattering data were collected at the BM29 beamline (European Synchrotron Radiation Facility, Grenoble, France) equipped with a Pilatus 1M detector (45). Data collection and data analysis are detailed in the supporting information. Figures and selected models to be compared with SAXS data were generated using PyMOL. The interactive visualization and analysis of the density maps based on the *ab initio* model (DAMFILT) were performed with the program UCSF Chimera (46).

Surface plasmon resonance–based experiments

SPR measurements were performed using a Biacore X100 instrument (GE Healthcare) as detailed in the supporting information.

Enzymatic assay for NAMPT and GAPDH activity

The mixtures of pure NAMPT (8 μg/ml) and NAMPT 5xMut (8 μg/ml) in their free form, in complex with GAPDH (270 nM) and the substrate nicotinamide, were incubated at 37 °C for 60 min, and the product NMN was measured as described previously (47) using a Spark 20M multimode microplate reader (Tecan).

The reaction buffer contained 0.4 mM phosphoribosyl pyrophosphate, 2 mM ATP, 2 mM DTT, 12 mM $MgCl_2$, and 50 mM Tris-HCl (pH 7.5) and increasing concentrations of NAM from 50 to 0.625 μM. The amount of NMN produced by the enzyme in the incubation time was calculated with a calibration curve for the fluorescence intensity of an aqueous solution of NMN at a known concentration.

GAPDH (0.04 μg/ml) activity was tested by a spectrophotometric assay (Tecan Sunrise) monitoring the absorbance at 340 nm of NADH (6220 M^{-1} cm^{-1}) at 25 °C. The analysis was performed in the absence and in the presence of NAMPT (0.5 μM) and NAMPT 5xMut (0.5 μM), respectively. The reaction mixture contained 1 mM NAD^+, 50 mM phosphate buffer, pH 7.5, and increasing concentrations of G3P from 300 to 1.2 μM. Kinetic parameters were calculated as described previously (48), using a nonlinear least-square fit of the data using the Sigma Plot Enzyme Kinetics Module 1.3 (Systat Software, San Jose, CA). NMN and G3P data were fitted with the Michaelis–Menten equation for hyperbolic substrate kinetics (Table S1).

MS analyses

The peptide mixture was analyzed by LC-MS/MS analysis using a Dionex Ultimate 3000 ultra-HPLC system (Thermo Scientific) coupled to an Orbitrap-Fusion-Tribrid mass spectrometer (Thermo Scientific) with a Phoenix Nimbus (Phoenix S&T) ion source. Sample preparations and data from LC-MS/MS analysis are described in the supporting information. The proteomics data of the MS experiments are available from the MassIVE data repository (https://massive.ucsd.edu)[5] with the data set identifier MSV000084426. All protein identifications and all cross-linked peptides identified are reported in the supporting Excel file, tables_LCMS_analysis.xlsx.

NAMPT$_2$-GAPDH complex prediction and peptide design

The homodimeric structure of NAMPT (PDB code 5U2M) (22) and the monomeric structure of GAPDH (PDB code 5C7I)

[5] Please note that the JBC is not responsible for the long-term archiving and maintenance of this site or any other third party hosted site.

(23) with the best X-ray resolution were selected from the PDB and used to predict the three-dimensional organization of the NAMPT2-GAPDH complex by using a standard protein-protein docking approach. 200 runs of docking were performed using the web version of the Haddock software 23. We decided to use Haddock because this software was already demonstrated to be particularly suitable for protein-DNA and protein-protein docking (49, 50). No *a priori* information concerning the regions and the residues of both proteins (*i.e.* NAMPT and GAPDH) directly involved in the complex assembly were available, and for this reason, we used the C-Port software (25). The best NAMPT2-GAPDH complex was chosen by considering the Haddock score, which is estimated according to the weighted sum of several energy terms: van der Waals, electrostatic, dihedral angle restraints, symmetry restraints, diffusion anisotropy, buried surface area, and binding and desolvation energies (26). The selected complex was then use to identify the type and the number of interactions that mainly stabilized the NAMPT2-GAPDH complex to select the GAPDH regions more suitable for the design of different peptides able to inhibit the complex formation. Specifically, four peptides were designed (*i.e.* G1–G4) joining different small unstructured regions of GAPDH that were observed in the predicted complex to be inserted with high geometric and chemo-physical complementarity between the NAMPT homodimer interface. The peptide synthesis is described in detail in the supporting information.

Reagents

H_2O_2 was from Marco Viti Farmaceutici (Como, Italy); *S*-nitrosoglutathione GSNO N4148 was from Sigma; etoposide E1383 was from Sigma; cisplatin BP809 was from Sigma; and Omigapil (CGP 3466B maleate) sc-361137 was from Santa Cruz Biotechnology, Inc. UV radiation was from a UV lamp at 254 nm.

Antibodies

Antibodies used were as follows: mouse (Mo) anti-NAMPT from AdipoGen (OMNI379); rabbit (Rb) anti-NAMPT GTX128973 from GeneTex; Mo anti-actin A1978 from Sigma; Rb anti-GAPDH G9545 from Sigma; Mo anti-GAPDH (1D4) from Novus Biologicals (NB300-221); Mo anti-phosphohistone H2A (Ser^{139}) clone JBW301 from Millipore; Rb anti-H2A ab18255 from Abcam; and Rb anti-FLAG F7425 from Sigma. Secondary antibodies for immunofluorescence were as follows: Alexa Fluor 555 goat anti-rabbit (IS-20232, Immune Sciences); Alexa Fluor 555 donkey anti-mouse (A-31570, Invitrogen); and Alexa Fluor 488 chicken anti-rabbit (A-21441, Invitrogen). The DRQ5 fluorescent probe solution for nuclear staining was from Invitrogen (catalog no. 62251).

Statistical analysis

Data are presented as mean ± S.E. The normality of data distributions was assessed using the Shapiro–Wilk test. Parametric (unpaired *t* test and one-way analysis of variance) or nonparametric (Mann–Whitney *U* test and one-way Kruskal–Wallis *H* test) statistical analysis was used for comparisons of data. All statistical assessments were two-sided, and a value of $p < 0.05$ was considered statistically significant. Statistical analysis was performed using GraphPad Prism software (GraphPad Software, Inc.). *n* (number of independent experiments, defined as experiments performed on different days) is reported in the respective figure legends.

Author contributions—A. A. Grolla, D. D. M., J. A. W., R. M., A. A. Genazzani, and S. G. conceptualization; A. A. Grolla, R. M., C. A., X. F., and C. T. data curation; A. A. Grolla, R. M., D. D. M., G. O., F. G., and S. D. formal analysis; A. A. Grolla, R. M., D. D. M., M. B., A. G., G. O., F. G., U. G., E. D. G., F. M., C. A., M. G., S. T., M. C., X. F., G. C., C. T., F. R., E. A., J. A. W., S. D., M. R., and S. G. methodology; A. A. Grolla, A. A. Genazzani, and S. G. writing-original draft; A. A. Grolla, A. A. Genazzani, and S. G. project administration; R. M., D. D. M., M. B., F. G., E. D. G., S. T., J. A. W., and M. R. software; R. M., M. B., G. O., and U. G. validation; D. D. M., A. G., G. O., U. G., F. M., G. C., J. A. W., S. D., M. R., and S. G. resources; S. B. investigation; C. T., J. A. W., M. R., A. A. Genazzani, and S. G. supervision; S. G. and A. A. Genazzani funding acquisition.

Acknowledgments—We thank Nestor Santiago, Nausicaa Clemente, and Antonella Vallario for invaluable technical help with experiments. We acknowledge the HIS Mouse Facility of the Academic Medical Center, Amsterdam and the Bloemenhove Clinic (Heemstede, The Netherlands) for providing fetal tissues.

References

1. Goodman, R. P., Calvo, S. E., and Mootha, V. K. (2018) Spatiotemporal compartmentalization of hepatic NADH and NADPH metabolism. *J. Biol. Chem.* **293,** 7508–7516 CrossRef Medline
2. Pollak, N., Dölle, C., and Ziegler, M. (2007) The power to reduce: pyridine nucleotides–small molecules with a multitude of functions. *Biochem. J.* **402,** 205–218 CrossRef Medline
3. Busso, N., Karababa, M., Nobile, M., Rolaz, A., Van Gool, F., Galli, M., Leo, O., So, A., and De Smedt, T. (2008) Pharmacological inhibition of nicotinamide phosphoribosyltransferase/visfatin enzymatic activity identifies a new inflammatory pathway linked to NAD. *PLoS ONE* **3,** e2267 CrossRef Medline
4. Houtkooper, R. H., Cantó, C., Wanders, R. J., and Auwerx, J. (2010) The secret life of NAD$^+$: an old metabolite con- trolling new metabolic signaling pathways. *Endocr. Rev.* **31,** 194–223 CrossRef Medline
5. Magni, G., Amici, A., Emanuelli, M., Orsomando, G., Raffaelli, N., and Ruggieri, S. (2004) Enzymology of NAD$^+$ homeostasis in man. *Cell Mol. Life Sci.* **61,** 19–34 CrossRef Medline
6. Gibson, B. A., and Kraus, W. L. (2012) New insights into the molecular and cellular functions of poly(ADP-ribose) and PARPs. *Nat. Rev. Mol. Cell Biol.* **13,** 411–424 CrossRef Medline
7. Lee, H. C. (2012) Cyclic ADP-ribose and nicotinic acid adenine dinucleotide phosphate (NAADP) as messengers for calcium mobilization. *J. Biol. Chem.* **287,** 31633–31640 CrossRef Medline
8. Essuman, K., Summers, D. W., Sasaki, Y., Mao, X., DiAntonio, A., and Milbrandt, J. (2017) The SARM1 Toll/interleukin-1 receptor domain possesses intrinsic NAD$^+$ cleavage activity that promotes pathological axonal degeneration. *Neuron* **93,** 1334–1343.e5 CrossRef Medline
9. Dali-Youcef, N., Lagouge, M., Froelich, S., Koehl, C., Schoonjans, K., and Auwerx, J. (2007) Sirtuins: the "magnificent seven", function, metabolism and longevity. *Ann. Med.* **39,** 335–345 CrossRef Medline
10. Rongvaux, A., Andris, F., Van Gool, F., and Leo, O. (2003) Reconstructing eukaryotic NAD metabolism. *BioEssays* **25,** 683–690 CrossRef Medline
11. Opitz, C. A., and Heiland, I. (2015) Dynamics of NAD-metabolism: everything but constant. *Biochem. Soc. Trans.* **43,** 1127–1132 CrossRef Medline
12. Mori, V., Amici, A., Mazzola, F., Di Stefano, M., Conforti, L., Magni, G., Ruggieri, S., Raffaelli, N., and Orsomando, G. (2014) Metabolic profiling of

alternative NAD biosynthetic routes in mouse tissues. *PLoS ONE* **9,** e113939 CrossRef Medline

13. Revollo, J. R., Grimm, A. A., and Imai, S. (2004) The NAD biosynthesis pathway mediated by nicotinamide phosphoribosyltransferase regulates Sir2 activity in mammalian cells. *J. Biol. Chem.* **279,** 50754–50763 CrossRef Medline
14. Rongvaux, A., Galli, M., Denanglaire, S., Van Gool, F., Drèze, P. L., Szpirer, C., Bureau, F., Andris, F., and Leo, O. (2008) Nicotinamide phosphoribosyl transferase/pre-B cell colony-enhancing factor/visfatin is required for lymphocyte development and cellular resistance to genotoxic stress. *J. Immunol.* **181,** 4685–4695 CrossRef Medline
15. Zhai, R. G., Rizzi, M., and Garavaglia, S. (2009) Nicotinamide/nicotinic acid mononucleotide adenylyltransferase, new insights into an ancient enzyme. *Cell Mol. Life Sci.* **66,** 2805–2818 CrossRef Medline
16. Grolla, A. A., Travelli, C., Genazzani, A. A., and Sethi, J. K. (2016) Extracellular nicotinamide phosphoribosyltransferase, a new cancer metabokine. *Br. J. Pharmacol.* **173,** 2182–2194 CrossRef Medline
17. Audrito, V., Managò, A., Gaudino, F., and Deaglio, S. (2020) Targeting metabolic reprogramming in metastatic melanoma: the key role of nicotinamide phosphoribosyltransferase (NAMPT). *Semin. Cell Dev. Biol.* **98,** 192–201 CrossRef Medline
18. Kitani, T., Okuno, S., and Fujisawa, H. (2003) Growth phase-dependent changes in the subcellular localization of pre-B-cell colony-enhancing factor. *FEBS Lett.* **544,** 74–78 CrossRef Medline
19. Svoboda, P., Krizova, E., Sestakova, S., Vapenkova, K., Knejzlik, Z., Rimpelova, S., Rayova, D., Volfova, N., Krizova, I., Rumlova, M., Sykora, D., Kizek, R., Haluzik, M., Zidek, V., Zidkova, J., and Skop, V. (2019) Nuclear transport of nicotinamide phosphoribosyltransferase is cell cycle-dependent in mammalian cells, and its inhibition slows cell growth. *J. Biol. Chem.* **294,** 8676–8689 CrossRef Medline
20. Yang, H., Yang, T., Baur, J. A., Perez, E., Matsui, T., Carmona, J. J., Lamming, D. W., Souza-Pinto, N. C., Bohr, V. A., Rosenzweig, A., de Cabo, R., Sauve, A. A., and Sinclair, D. A. (2007) Nutrient-sensitive mitochondrial NAD$^+$ levels dictate cell survival. *Cell* **130,** 1095–1107 CrossRef Medline
21. Tristan, C., Shahani, N., Sedlak, T. W., and Sawa, A. (2011) The diverse functions of GAPDH: views from different subcellular compartments. *Cell. Signal.* **23,** 317–323 CrossRef Medline
22. Wilsbacher, J. L., Cheng, M., Cheng, D., Trammell, S. A. J., Shi, Y., Guo, J., Koeniger, S. L., Kovar, P. J., He, Y., Selvaraju, S., Heyman, H. R., Sorensen, B. K., Clark, R. F., Hansen, T. M., Longenecker, K. L., *et al.* (2017) Discovery and characterization of novel nonsubstrate and substrate NAMPT inhibitors. *Mol. Cancer Ther.* **16,** 1236–1245 CrossRef Medline
23. Danshina, P. V., Qu, W., Temple, B. R., Rojas, R. J., Miley, M. J., Machius, M., Betts, L., and O'Brien, D. A. (2016) Structural analyses to identify selective inhibitors of glyceraldehyde 3-phosphate dehydrogenase-S, a sperm-specific glycolytic enzyme. *Mol. Hum. Reprod.* **22,** 410–426 CrossRef Medline
24. Tisdale, E. J. (2002) Glyceraldehyde-3-phosphate dehydrogenase is phosphorylated by protein kinase Cι/λ and plays a role in microtubule dynamics in the early secretory pathway. *J. Biol. Chem.* **277,** 3334–3341 CrossRef Medline
25. Mansur, N. R., Meyer-Siegler, K., Wurzer, J. C., and Sirover, M. A. (1993) Cell cycle regulation of the glyceraldehyde-3-phosphate dehydrogenase/uracil DNA glycosylase gene in normal human cells. *Nucleic Acids Res.* **21,** 993–998 CrossRef Medline
26. van Zundert, G. C. P., Rodrigues, J. P. G. L. M., Trellet, M., Schmitz, C., Kastritis, P. L., Karaca, E., Melquiond, A. S. J., van Dijk, M., de Vries, S. J., Bonvin, A. M. J. J. (2016) The HADDOCK2.2 web server: user-friendly integrative modeling of biomolecular complexes. *J. Mol. Biol.* **428,** 720–725 Medline
27. de Vries, S. J., and Bonvin, A. M. (2011) CPORT: a consensus interface predictor and its performance in prediction-driven docking with HADDOCK. *PLoS ONE* **6,** e17695 CrossRef Medline
28. Bockwoldt, M., Houry, D., Niere, M., Gossmann, T. I., Reinartz, I., Schug, A., Ziegler, M., and Heiland, I. (2019) Identification of evolutionary and kinetic drivers of NAD-dependent signaling. *Proc. Natl. Acad. Sci.* **116,** 15957–15966 CrossRef Medline
29. Donini, S., Ferraris, D. M., Miggiano, R., Massarotti A, and Rizzi, M. (2017) Structural investigations on orotate phosphoribosyltransferase from *Mycobacterium tuberculosis*, a key enzyme of the *de novo* pyrimidine biosynthesis. *Sci. Rep.* **7,** 1180 CrossRef Medline
30. Maldi, E., Travelli, C., Caldarelli, A., Agazzone, N., Cintura, S., Galli, U., Scatolini, M., Ostano, P., Miglino, B., Chiorino, G., Boldorini, R., and Genazzani, A. A. (2013) Nicotinamide phosphoribosyltransferase (NAMPT) is over-expressed in melanoma lesions. *Pigment Cell Melanoma Res.* **26,** 144–146 CrossRef Medline
31. Sawa, A., Khan, A. A., Hester, L. D., and Snyder, S. H. (1997) Glyceraldehyde-3-phosphate dehydrogenase: nuclear translocation participates in neuronal and nonneuronal cell death. *Proc. Natl. Acad. Sci. U.S.A.* **94,** 11669–11674 CrossRef Medline
32. Hou, X., Snarski, P., Higashi, Y., Yoshida, T., Jurkevich, A., Delafontaine, P., and Sukhanov, S. (2017) Nuclear complex of glyceraldehyde-3-phosphate dehydrogenase and DNA repair enzyme apurinic/apyrimidinic endonuclease I protect smooth muscle cells against oxidant-induced cell death. *FASEB J.* **31,** 3179–3192 CrossRef Medline
33. Kornberg, M. D., Sen, N., Hara, M. R., Juluri, K. R., Nguyen, J. V., Snowman, A. M., Law, L., Hester, L. D., and Snyder, S. H. (2010) GAPDH mediates nitrosylation of nuclear proteins. *Nat. Cell Biol.* **12,** 1094–1100 CrossRef Medline
34. Hara, M. R., Agrawal, N., Kim, S. F., Cascio, M. B., Fujimuro, M., Ozeki, Y., Takahashi, M., Cheah, J. H., Tankou, S. K., Hester, L. D., Ferris, C. D., Hayward, S. D., Snyder, S. H., and Sawa, A. (2005) *S*-Nitrosylated GAPDH initiates apoptotic cell death by nuclear translocation following Siah1 binding. *Nat. Cell Biol.* **7,** 665–674 CrossRef Medline
35. Hara, M. R., Thomas, B., Cascio, M. B., Bae, B. I., Hester, L. D., Dawson, V. L., Dawson, T. M., and Sawa, A., and Snyder S. H. (2006) Neuroprotection by pharmacologic blockade of the GAPDH death cascade. *Proc. Natl. Acad. Sci. U.S.A.* **103,** 3887–3889 CrossRef Medline
36. Zheng, L., Roeder, R. G., and Luo, Y. (2003) Phase activation of the histone H2B promoter by OCA-S, a coactivator complex that contains GAPDH as a key component. *Cell* **114,** 255–266 CrossRef Medline
37. Ryu, K. W., Nandu, T., Kim, J., Challa, S., DeBerardinis, R. J., and Kraus, W. L. (2018) Metabolic regulation of transcription through compartmentalized NAD$^+$ biosynthesis. *Science* **360,** eaan5780 CrossRef Medline
38. Cambronne, X. A., Stewart, M. L., Kim, D., Jones-Brunette, A. M., Morgan, R. K., Farrens, D. L., Cohen, M. S., and Goodman, R. H. (2016) Biosensor reveals multiple sources for mitochondrial NAD$^+$. *Science* **352,** 1474–1477 CrossRef Medline
39. Gaudino, F., Manfredonia, I., Managò, A., Audrito, V., Raffaelli, N., Vaisitti, T., and Deaglio, S. (2019) Subcellular characterization of nicotinamide adenine dinucleotide biosynthesis in metastatic melanoma by using organelle-specific biosensors. *Antioxid. Redox Signal.* **31,** 1150–1165 CrossRef Medline
40. Nikiforov, A., Kulikova, V., and Ziegler, M. (2015) The human NAD metabolome: functions, metabolism and compartmentalization. *Crit. Rev. Biochem. Mol. Biol.* **50,** 284–297 CrossRef Medline
41. Sirover, M. A. (2017) GAPDH. In *Moonlighting Proteins* (Henderson, B., ed) pp. 147–167, Wiley, New York
42. Grolla, A. A., Torretta, S., Gnemmi, I., Amoruso, A., Orsomando, G., Gatti, M., Caldarelli, A., Lim, D., Penengo, L., Brunelleschi, S., Genazzani, A. A., and Travelli, C. (2015) Nicotinamide phosphoribosyltransferase (NAMPT/PBEF/visfatin) is a tumoural cytokine released from melanoma. *Pigment Cell Melanoma Res.* **28,** 718–729 CrossRef Medline
43. Buonvicino, D., Mazzola, F., Zamporlini, F., Resta, F., Ranieri, G., Camaioni, E., Muzzi, M., Zecchi, R., Pieraccini, G., Dölle, C., Calamante, M., Bartolucci, G., Ziegler, M., Stecca, B., Raffaelli, N., and Chiarugi, A. (2018) Identification of the nicotinamide salvage pathway as a new toxification route for antimetabolites. *Cell Chem. Biol.* **25,** 471–482.e7 CrossRef Medline
44. Amici, A., Grolla, A. A., Del Grosso, E., Bellini, R., Bianchi, M., Travelli, C., Garavaglia, S., Sorci, L., Raffaelli, N., Ruggieri, S., Genazzani, A. A., and Orsomando, G. (2017) Synthesis and degradation of adenosine 5′-tetraphosphate by nicotinamide and nicotinate phosphoribosyltransferases. *Cell Chem. Biol.* **24,** 553–564.e4 CrossRef Medline

45. Round, A., Felisaz, F., Gobbo, A., Huet, J., Fodinger, L., Villard, C., Pernot, P., McSweeney, S., Blanchet, C. E., Roessle, M., Svergun, D. I., and Cipriani, F. (2015) BioSAXS sample changer: a robotic sample changer for rapid and reliable high-throughput X-ray solution scattering. *Acta Crystallogr. D Biol. Crystallogr.* **71,** 67–75 CrossRef Medline
46. Pettersen, E. F., Goddard, T. D., Huang, C. C., Couch, G. S., Greenblatt, D. M., Meng, E. C., and Ferrin, T. E. (2004) UCSF Chimera: a visualization system for exploratory research and analysis. *J. Comput. Chem.* **25,** 1605–1612 CrossRef Medline
47. Zhang, R. Y., Qin, Y., Lv, X. Q., Wang, P., Xu, T. Y., Zhang, L., and Miao, C. Y. (2011) A fluorometric assay for high-throughput screening targeting nicotinamide phosphoribosyltransferase. *Anal. Biochem.* **412,** 18–25 CrossRef Medline
48. Donini, S., Garavaglia, S., Ferraris, D. M., Miggiano, R., Mori, S., Shibayama, K., and Rizzi, M. (2017) Biochemical and structural investigations on phosphoribosylpyrophosphate synthetase from *Mycobacterium smegmatis*. *PLoS ONE* **12,** e0175815 CrossRef Medline
49. Di Marino, D., Chillemi, G., De Rubeis, S., Tramontano, A., Achsel, T., and Bagni, C. (2015) MD and docking studies reveal that the functional switch of CYFIP1 is mediated by a butterfly-like motion. *J. Chem. Theory Comput.* **11,** 3401–3410 CrossRef Medline
50. Di Marino, D., Achsel, T., Lacoux, C., Falconi, M., and Bagni, C. (2014) Molecular dynamics simulations show how the FMRP Ile304Asn mutation destabilizes the KH2 domain structure and affects its function. *J. Biomol. Struct. Dyn.* **32,** 337–350 CrossRef Medline